Sensitivity of Tropical Cyclones to Parameterized Convection in the NASA GEOS5 Model

Young-Kwon Lim[1,2], Siegfried D. Schubert[1], Oreste Reale[3,4], Myong-In Lee[6], Andrea M. Molod[1,5], Max J. Suarez[1]

Corresponding author: Young-Kwon Lim (Young-Kwon.Lim@nasa.gov)

[1]Bldg. 33, code 610.1, 8800 Greenbelt Rd.,
Global Modeling and Assimilation Office, NASA/GSFC, Greenbelt, Maryland, 20771
[2]Goddard Earth Sciences Technology and Research, I. M. System Group
[3]Earth Science Division, Atmospheres, NASA/GSFC, Greenbelt, Maryland
[4]Goddard Earth Sciences Technology and Research,
Universities Space Research Association (USRA)
[5]ESSIC, University of Maryland, College Park, Maryland
[6]Ulsan Institute of Science and Technology (UNIST), Ulsan, South Korea

February 03, 2014
Submitted to Journal of Climate

Abstract

The sensitivity of tropical cyclones (TCs) to changes in parameterized convection is investigated to improve the simulation of TCs in the North Atlantic. Specifically, the impact of reducing the influence of the Relaxed Arakawa-Schubert (RAS) scheme-based parameterized convection is explored using the Goddard Earth Observing System version5 (GEOS5) model at 0.25° horizontal resolution. The years 2005 and 2006 characterized by very active and inactive hurricane seasons, respectively, are selected for simulation.

A reduction in parameterized deep convection results in an increase in TC activity (e.g., TC number and longer life cycle) to more realistic levels compared to the baseline control configuration. The vertical and horizontal structure of the strongest simulated hurricane shows the maximum lower-level (850-950hPa) wind speed greater than 60 m/s and the minimum sea level pressure reaching ~940mb, corresponding to a category 4 hurricane - a category never achieved by the control configuration. The radius of the maximum wind of ~50km, the location of the warm core exceeding 10°C, and the horizontal compactness of the hurricane center are all quite realistic without any negatively affecting the atmospheric mean state.

This study reveals that an increase in the threshold of minimum entrainment suppresses parameterized deep convection by entraining more dry air into the typical plume. This leads to cooling and drying at the mid- to upper-troposphere, along with the positive latent heat flux and moistening in the lower-troposphere. The resulting increase in conditional instability provides an environment that is more conducive to TC vortex development and upward moisture flux convergence by dynamically resolved moist convection, thereby increasing TC activity.

1. Introduction

This article is inspired by a recent research on tropical cyclone (TC) simulation coordinated by the US CLIVAR hurricane working group (http://www.usclivar.org/working-groups/hurricane) Among various science issues raised in the research, it was found that many current general circulation models (GCMs) seriously underestimate tropical cyclone (TC) activity over the North Atlantic when run at ~0.5 degree latitude/longitude or coarser horizontal resolution as opposed to some other basins such as the North Pacific (Walsh et al. 2013; Shaevitz et al. 2014). Only a few recent GCMs simulate TC activity in the North Atlantic with some success (e.g., Zhao et al. 2009). A question is raised on whether horizontal resolution finer than ~0.5 degree is necessary to achieve reasonable TC numbers over the North Atlantic, even though resolution appears less critical for simulating TC numbers than the intensity (Strachan et al. 2013). Compared to TC numbers, simulating realistic TC intensity and spatial structure appears more unattainable at these resolutions (~0.5 degree or coarser), with generally weak and poorly organized systems occurring in all the GCMs (more than 10) involved in the working group. Higher resolution may be more appropriate to allow for a better representation of African easterly waves and the associated strong low-level vorticity, leading to more realistic simulation of Atlantic TC activity including number, intensity, life-cycle and spatial structure (Knutson et al. 2007; Caron et al. 2011; Putman and Suarez 2011; Daloz et al. 2012; Emanuel 2013).

Several previous studies have identified deficiencies in the simulation of moist convective processes as substantially affecting the ability to simulate TC characteristics (Slingo et al. 1994; Zhang and McFarlane 1995; Smith 2000; Benjamin et al. 2008; Zhao et al. 2012). Smith (2000) suggests that major improvements in TC predictions will depend on improvements in the

representation of convection in hurricane models. Knutson et al. (2004), Atlas et al. (2005), LaRow et al. (2008), Ma and Tan (2009) and Reed and Jablonowski (2011) performed model experiments to examine the sensitivity of the global TC numbers to changes in the convective parameterizations. Shen et al. (2006) and Stan (2012) examined the impact of disabling the convective parameterizations (in particular the schemes developed by Arakawa and Schubert (1974) and Moorthi and Suarez (1992)) on GCM hurricane forecasts. Both studies agreed on that explicit representation of cloud processes produces a larger number of TC events, with stronger intensity and longer life-cycles (Reed and Jablonowski 2011; Stan 2012). However, the details of the atmospheric processes responsible for altering TC activity were not the focus of the above studies. Some of the atmospheric responses to changes in deep convective activity are discussed in Zhao et al. (2012), which focuses on the impacts on vertical velocity, temperature and humidity. That study identifies stronger sensitivity of mid-tropospheric vertical motion to the minimum entrainment compared with the other variables (humidity and vertical wind shear): the importance of the response of vertical motion is also discussed in Oouchi et al. (2006).

The sensitivity of the atmospheric response to the convective parameterization and its impact on TC activity motivates the current study to improve the simulation of TC activity over the North Atlantic in GCMs. As in Tokioka et al. (1988), Held et al. (2007) and Kang et al. (2008), we find that increasing the threshold of minimum entrainment rate makes the convective plume entrain more dry air as it ascends, losing in-cloud buoyancy more rapidly when entraining. As a result, deep convection is inhibited from occurring in updrafts with a lateral entrainment rate λ lower than a threshold value λ_0 (Tokioka et al. 1988; Held et al. 2007). Parameterized deep convection, including the sub-grid scale cloud representation is restricted by increasing λ_0 (Held et al. 2007; Kang et al. 2008), while the fraction of large-scale condensation by non-

92 convective clouds increases through the large-scale cloud/condensation module (Tiedtke 1993)
93 as opposed to the convection module (Kang et al. 2008). Wang (2014) found that this non-deep
94 convection plays a role in moistening the lower to middle troposphere whereas deep convection
95 moistens the upper-troposphere. Zhao et al. (2012) also found that an inhibition of the convective
96 parameterization through enhanced lateral mixing into convective plumes leads to increased TC
97 genesis, along with a colder and drier upper troposphere.

98 The main objective of this study is to improve the simulation of North Atlantic TC activity
99 in the National Aeronautics and Space Administration (NASA) Goddard Earth Observing
100 System Version 5 (GEOS-5) model (Rienecker et al. 2008; Molod et al. 2012), including the TC
101 number, intensity, life cycle and horizontal/vertical structures. We focus on the cumulus
102 entrainment rate in the GEOS-5 model run at a relatively high horizontal resolution (0.25 degree)
103 to determine the thresholds of minimum entrainment that reliably reproduce the TC activity over
104 the North Atlantic. An important aspect of this study is that we also focus on maintaining a
105 realistic mean climate state – an aspect of the simulations (the response of the mean state to the
106 changes in deep convection) many previous studies have not emphasized. The analysis of the
107 runs is geared to better understanding the atmospheric response determining the TC activity over
108 the North Atlantic with a particular focus on the atmospheric instability over the TC genesis
109 region, the thermodynamic and radiative balance, the low-level fluxes and circulation, and the
110 mean climate state response.

111 The organization of the paper is as follows. Section 2 describes the GEOS-5 model and the
112 experimental design. The results of the sensitivity experiments are presented in Section 3,
113 including TC numbers, intensity, life cycle and spatial structure of the strongest hurricanes. We
114 investigate in Section 4 the relevant atmospheric dynamics and physics to explain the TC activity

115 changes that occur as a result of the modifications to the parameterized deep convection. Some
116 verification of the atmospheric basic state changes due to the deep convection changes is also
117 provided in Section 4, followed by concluding remarks and discussion in Section 5.
118
119 2. Model and Experimental design
120 2.1 Model
121 We utilize the NASA GEOS-5 model (Rienecker et al. 2008; Molod et al. 2012) for our
122 experiments. The model is run with 72 hybrid-sigma vertical levels, extending to 0.01 hPa, and
123 ~0.25° latitude/longitude horizontal resolution. The convection scheme in the GEOS5 model is
124 basically a modified version of the Relaxed Arakawa Schubert (RAS) scheme of Moorthi and
125 Suarez (1992). In the modified version, multiple convective plumes in RAS have the convection
126 base level at the top of the planetary boundary layer. The adjustment time scale of plumes is a
127 function of the vertical depth of plumes, which varies from 0.5 hr for the shallowest plume to 12
128 hr for the deepest. Another major modification to RAS, which affects convective variability of
129 the model substantially and hence the intensity of simulated TCs, is the stochastic determination
130 of the minimum entrainment threshold. This is basically same as in Tokioka et al. (1988), which
131 modification is known as limiting frequent adjustment of deep convection in a model and
132 increasing the variability of deep convection (Lee et al. 2003; Lin et al. 2008). For "Tokioka"
133 constraint in this study, the threshold value is non-deterministic so that the subsequent value is
134 determined randomly with a predetermined power function:
135 $$\lambda_0 = \frac{\alpha}{D} x^n, \quad 0 \le x \le 1 \qquad (1)$$
136 where α is a free parameter, D the depth of the subcloud layer, and x a random number chosen at
137 every model integration time step. Here the depth of the subcloud layer D is assumed to be

138 related with the plume radius by Simpson and Wiggert (1969), and this stochastic determination
139 has a basis to consider spatial statistics of the observed cloud widths (or radius) and volumes that
140 follow a power law distribution found by Bacmeister and Stephens (2011) from the CloudSat
141 data (Stephens et al. 2002). Figure 1 compares the minimum entrainment threshold values
142 between the conventional, deterministic method from Tokioka et al. (1988) and the stochastic
143 method in this study. In case of n=1/2, which is used in this study, the threshold curve increases
144 with the square root function (Fig. 1), and restores to the conventional Tokioka constraint. This
145 tends to impose restriction on the entrainment rate in most cases, but occasionally allowing a
146 very deep and less entraining convection plumes. Putman and Suarez (2011) used the same
147 version of GEOS-5 that used in this study for their tropical cyclone simulation, but with much
148 higher horizontal resolution of ~7km.
149 Increase in the Tokioka constraint (i.e., increase in the threshold of minimum entrainment)
150 makes more difficult condition for sub-grid scale deep convection. While the parameterized deep
151 convective process is suppressed as a result of this Tokioka constraint, resolved-scale non-
152 convective clouds are favored and thus, more active large-scale cloud/condensation and
153 precipitation process becomes feasible.
154
155 2.2 Experimental design
156 Three types of experiments are carried out by applying different Tokioka constraints in
157 model simulations of the years 2005 and 2006, which are very active and inactive hurricane
158 years, respectively. We call these three experiments A, B, and C. Experiment A (ExpA) has the
159 strongest Tokioka constraint, where the greatest possibility of large thresholds of minimum
160 entrainment exists, while Experiment B corresponds to an intermediate range of thresholds

161 (ExpB), and Experiment C (ExpC), which is a baseline control run, corresponds to the lowest
162 minimum entrainment range that allows more parameterized deep convection relative to the
163 ExpA and ExpB. These were implemented in the model with the minimum $\alpha/D = 2\ km^{-1}$ (ExpA),
164 $0.7\ km^{-1}$(ExpB), and $0.45\ km^{-1}$ (ExpC), respectively in Equation (1). Please note that solid curve
165 as a bottom line for minimum entrainments in Fig. 1 can vary with the α/D values given in each
166 experiment. The curve for ExpA is placed above the other two curves (for ExpB and ExpC),
167 while the opposite is true for the curve for ExpC. Although the choice of n in Equation (1) can
168 affect the results, but this is left for future sensitivity study. As mentioned earlier, the horizontal
169 resolution is a quarter-degree latitude/longitude. The minimum entrainment thresholds is
170 increased in our experiments (e.g., ExpA and ExpB) to identify the model sensitivity in
171 simulating TCs with a focus on better performance across the Atlantic basin. From the above
172 experiments, we intend to estimate the best Tokioka constraint as determined by the
173 improvements in TC simulation including genesis, lifetime, track and intensity at this resolution.
174 Each type of experiments consists of three ensemble members. All simulations are done with
175 prescribed weekly sea surface temperature (SST) forcing (the HadISST of Rayner et al. 2003),
176 and are initialized from Modern-Era Retrospective Analysis for Research and Applications
177 (MERRA, Rienecker et al. 2011) data on May 1 each year.
178
179 3. Sensitivity of TC characteristics to changes in parameterized deep convection
180 TCs are detected for each year (2005 and 2006) and each experiment (ExpA, ExpB and
181 ExpC). The number of detected tropical storms and hurricanes is shown in Table 1. The basic
182 algorithm of TC detection and tracking is the same as that used in Vitart et al. (2003), Knutson et
183 al. (2007) and LaRow et al. (2008). Threshold values for wind speed, relative vorticity, warm

184 core, sea level pressure and minimum duration time are assigned in the algorithm to define TC
185 (Table 2) at a quarter degree resolution based on suggestions in Walsh et al. (2007). The
186 threshold values used here can be considered realistic because they are very close to the
187 thresholds to detect TCs from observational data. ExpA produces an excessive number of
188 tropical storms and hurricanes, compared with observations shown on the rightmost column
189 (Table 1). In particular, it produces too strong TC activity (hurricanes more than 20) even in
190 2006, which was recorded as a relatively calm hurricane year (Knapp et al. 2010). ExpB
191 produces more reasonable TC numbers, as they are closer to observations than either ExpA or
192 ExpC. ExpC shows generally weak TC activity and produces much weaker than observed TC
193 activity during the active hurricane season of 2005.

194 TC tracks are plotted for each experiment. During the 2005 season (Fig. 2), a variety of
195 tracks were observed: 1) Cap Verde-type TC systems that crossed the Atlantic making landfall
196 over the American continent, 2) early recurvers, 3) Gulf of Mexico TCs, and also 4) eastward
197 tracking systems embedded in the westerlies. Comparison between the experiments inidcates that
198 ExpA and ExpB both display a variety of tracks much larger than ExpC, and closer to the
199 observation. The results for 2006 (Fig. 3) show features similar to those obtained for 2005 in the
200 sense that the increased thresholds of minimum entrainment produce larger number of TCs with
201 longer life cycles and a track variety more similar to the observation over the Atlantic. This
202 model response is consistent with Emanuel et al. (2008) and Stan (2012), that showed a
203 sensitivity of TC activity to changes in the cumulus parameterization in the Community Climate
204 System Model (CCSM) (Gent et al. 2011).

205 Additional details of the model responses (including TC activity, TC intensity and vertical
206 hurricane structure) produced in each experiment are shown in Fig. 4 through 8. Scatter plots of

low-level (850-950hPa) wind versus SLP for 2005 (Fig. 4), show that the maximum wind speed is up to 61ms^{-1} in the ExpA, 60ms^{-1} in ExpB, and less than 60ms^{-1} in ExpC. The minimum SLP is down to 936, 943, and 963hPa, respectively in the three experiments. ExpA and ExpB reveal improved distributions of SLP and wind speed compared with ExpC. Note however that the observed wind speed is up to 80ms^{-1} and minimum SLP deeper than 920hPa for extremely strong hurricanes – something not reproduced by the model in any of the experiments. Much finer horizontal resolution (finer than 10km) such as that of Noda et al. (2012) and Putman and Suarez (2011) appear to be necessary for capturing such extremely strong hurricanes. The maximum wind speeds identified in ExpA and ExpB are comparable to those found in the idealized hurricane experiment of Reed and Jablonowski (2011). They simulated maximum wind speeds of ~60ms^{-1} at ~1km height and a quarter-degree horizontal resolution.

Figure 5 is the same as Fig. 4 but for 2006. The results show that the simulated wind speeds and minimum center SLP deepening for very strong hurricanes is comparable to or stronger than those for the observations (ExpA and ExpB). In contrast, ExpC exhibits weaker maximum wind and minimum SLP distribution compared with the observations.

The vertical structure of the strongest hurricane for ExpA is plotted in Fig. 6. The top left panel shows the wind speed (shaded) and temperature (contoured), and the right panel shows the warm core. The results for 2005 show a compact core and hurricane eye that is well defined. The maximum low level wind speeds (greater than 60ms^{-1}) and the radius of maximum winds (less than 50km) both correspond to very realistic TC representation. The warm core value is greater than 10°C and situated in the upper-troposphere, quite similar to the typical structure of observed hurricanes (Frank 1977). The bottom panel is the time series of the minimum SLP and maximum wind speed following the moving hurricane. The minimum SLP drops to 935hPa and maximum

wind speed reaches 61ms^{-1}. The main features for 2006 are quite similar to those found for 2005, showing a well-defined hurricane characterized by a maximum wind speed of 65ms^{-1} and minimum SLP of 935hPa.

The vertical structures of the strongest hurricanes in ExpB are shown in Fig. 7. Compared with ExpA, they are a little weaker, but still show a reasonable vertical structure in terms of compactness of the core, with the radius of the maximum wind less than ~50km (2 grid points in longitudinal direction), the maximum wind value near 60ms^{-1}, the minimum SLP of about 940hPa, and vertical profile of the warm core (reaching 10°C), which corresponds to a category 4 hurricane based on the Saffir-Simpson scale (http://www.nhc.noaa.gov/aboutsshws.php) in 2005. Observed wind .vs. SLP scatter plots in Figs. 4 and 5 indicated that the strongest observed hurricane in 2006 is weaker than that in 2005. The model reproduces well this difference between the two years (Fig. 7), but the difference is not as distinguishable as that found in the observation. As discussed in Fig. 4, the observed category 5 hurricane in 2005 was very hard to reproduce through a quarter-degree resolution run, resulting in rather a small difference in the intensity of the strongest hurricane between the two years in Fig. 7.

ExpC, which is the control run, also shows reasonable results (Fig. 8), though the storms are less organized than those found in the other two experiments. The warm core is weak with a value of approximately 6~8°C and located in the mid-troposphere. The wind speed, SLP, and sharpness of the hurricane core are also not as realistic as those in ExpA and ExpB. The weak hurricane structures found in ExpC are not inconsistent with the study of Vitart et al. (2001), which found that the vertical structures of hurricanes simulated by RAS tend to be less intense and have lower warm cores than those produced with moist convective adjustment (MCA) schemes (Manabe 1969), though the RAS scheme produces more TCs and higher relative

253 humidity than MCA schemes. In any event, the hurricane vertical structures shown in Fig. 6
254 through 8 provides compelling evidence that the suppression of parameterized deep convection
255 tends to produce more intense hurricanes with better organized vertical structures.
256
257 4. Atmospheric response to parameterized deep convection
258 The physical mechanisms by which the suppression of the cumulus parameterization
259 promotes TC activity are investigated next. The role of atmospheric moist static stability – a
260 factor known to affect TC characteristics (Smith 2000) is shown in Fig. 9, where the vertical
261 profile of moist static energy (left panel) and the vertical gradient of equivalent potential
262 temperature (right panel) are computed over the TC genesis region, which covers most of the
263 central and eastern tropical Atlantic (60°W~15°W, 5°N~20°N). Profiles from ExpA, ExpB, and
264 ExpC all exhibit a decrease with height in moist static energy at low levels (below 700~800hPa
265 height) and an increase at upper-levels, implying the possibility of conditional instability. The
266 ExpA result shows the possibility of stronger instability than ExpB and ExpC. The vertical
267 gradient of equivalent potential temperature ($-\frac{\partial \theta_e}{\partial p}$) (Fig. 9b) also shows that lower tropospheric
268 vertical column with the negative $-\frac{\partial \theta_e}{\partial p}$ is more extensive in Exp A than the other two
269 experiments, indicating the most unstable atmosphere occurs in ExpA, followed by ExpB and
270 ExpC.
271 The vertical temperature and humidity profiles are plotted over the TC genesis region in Fig.
272 10 to indicate how they are linked to the atmospheric instability. Here we plot the differences in
273 the vertical profiles of temperature/humidity between two experiments. The most striking
274 feature of these results is the mid- to upper-tropospheric cooling (Fig. 10a) and drying (Fig. 10b)
275 and lower-tropospheric moistening (Fig. 10b) resulting from the reduction in parameterized deep

276 convection. This vertical structure of the humidity is in good agreement with the results of Zhao
277 et al. (2012). With a larger threshold of minimum entrainment, it is not unexpected that more dry
278 air will be entrained into the plume, resulting in a drier upper atmosphere with decreased
279 buoyancy (Held et al. 2007). The reduction of in-cloud buoyancy leads to the suppression of
280 parameterized deep convection and less upper-tropospheric condensation heating. Figure 10
281 reflects such a change in the vertical profile of temperature and moisture, providing favorable
282 conditions for developing an unstable atmosphere. Upward moisture flux and dynamically
283 resolved convection are more likely to occur after the lower troposphere is moistened enough
284 (Wang 2014) under this unstable atmospheric condition.

285 Figure 11 shows the latent heating and evaporative flux with a focus on the near surface
286 moisture flux. We note that the differences between ExpB and ExpC exhibit very similar patterns
287 though with smaller magnitude (Figure not shown). Figure 11a shows that the latent heat flux is
288 significantly increased in ExpA throughout the Atlantic basin. The enhanced evaporative flux
289 from the ocean (Fig. 11b) gives rise to the increase in latent heat flux. We will see later (Fig. 12)
290 that the upward flux at the surface is also enhanced by increased ascending motion in the
291 unstable atmosphere. This is consistent with Zhao et al. (2012), who found that surface heat
292 fluxes including latent heat flux were influenced by vertical motion, and that this was important
293 for making the resolved-scale convection more favorable for tropical cyclone genesis.

294 Figures 11c quantifies the increase in conditional instability we inferred from Fig. 9 through
295 11b, in terms of the convective available potential energy (CAPE). It shows that CAPE is
296 significantly enhanced in ExpA (compared with the control) through the constraint on the
297 parameterized deep convection. CAPE exists within the conditionally unstable layer of the
298 troposphere, when a lifted parcel of air is warmer than the ambient air. It can be interpreted,

299 based on Fig. 10, that strong upper-tropospheric cooling overlying relatively warmer air at
300 lower-levels accompanied sufficient moisture, contributes to a build up of CAPE. The larger
301 CAPE in ExpA compared with the control run (ExpC) also demonstrates that dynamically
302 resolving convective processes would be enhanced with the suppression of parameterized deep
303 convection, resulting in an increase in large-scale condensation and precipitation (see the
304 fractional precipitation change in Fig. 15).

305 Figure 12a clearly illustrates the strong response of the vertical motion (see also Oouchi et al.
306 2006) to the unstable atmosphere caused by the restriction of parameterized deep convection.
307 The increase in atmospheric instability over the TC genesis region leads to increased ascending
308 motion throughout the vertical column with the largest increase occurring in ExpA, followed by
309 ExpB and then ExpC. The enhanced vertical ascent is associated with enhanced low-level
310 convergence (Fig. 13). This low-level convergence, combined with low-level moistening (Fig.
311 10) and positive latent heat flux (Fig. 11a), plays a role in increasing the moisture flux
312 convergence at low levels (Fig. 12b), with the largest values occurring in ExpA, followed by
313 ExpB and ExpC.

314 Figure 13 shows the distribution of the differences between ExpA and ExpC in some other
315 atmospheric quantities. The results show that low-level vorticity (850hPa), near-surface wind
316 variance (10m), low-level convergence (925hPa) and vertically integrated moisture flux
317 convergence are all enhanced over the eastern Atlantic. The enhancement is more pronounced
318 over the TC genesis region between about 10°N and 15°N (for genesis latitudes, see also Figs. 2
319 and 3). These spatial patterns emphasize once again that, as the parameterized deep convection is
320 suppressed through an increase in the minimum entrainment threshold, the resulting increase in

atmospheric instability makes dynamically resolved moist convection more active by enhancing low-level atmospheric motions (e.g., convergence, vorticity and wind variance).

To quantify that the atmospheric structures discussed so far provide a favorable TC genesis environment, we next calculate the genesis potential index (GPI). Here, the original version of GPI (Emanual and Nolan 2004) has been modified following Murakami et al. (2011) to include the influence of vertical motion in contributing to TC genesis. The modified GPI[1] is given by

$$\mathrm{GPI}=|10^5\eta|^{3/2}\left(\frac{RH}{50}\right)^3\left(\frac{V_{pot}}{70}\right)^3(1+0.1V_s)^{-2}\left(\frac{-\omega+0.1}{0.1}\right), \quad (2)$$

where η is the absolute vorticity at 850hPa level, RH is the relative humidity in percent at 850hPa, V_{pot} is the maximum potential intensity (MPI; m s^{-1}) defined in Emanuel (1995), V_s is the vertical wind shear (V(850hPa) minus V(200hPa)), and ω is the vertical wind velocity (Pa s^{-1}) at 500hPa. V_{pot} is modified by Bister and Emanuel (1998) from the original version of Emanuel (1995) so that

$$V_{pot}^2=\frac{C_kT_s}{C_dT_0}(CAPE^*-CAPE^b), \quad (3)$$

where C_k and C_d are the exchange coefficient for enthalpy and the drag coefficient, respectively. T_s is SST and T_0 is the mean outflow temperature. Two CAPE-related quantities, $CAPE^*$ and $CAPE^{\mathrm{b}}$ are the CAPE of the air displaced upward from saturation at sea level with reference to ambient air and the CAPE of the air at boundary layer, respectively.

The GPI formulation considers the influence of all the horizontal and vertical atmospheric structures and atmospheric instability discussed in reference to Fig. 9 through 13. As shown in Fig. 14, the GPI exhibits larger values in ExpA and ExpB than in the control run (ExpC). Large

[1] The source code for the FORTRAN version of the GPI calculation is available from ftp://texmex.mit.edu/pub/emanuel/TCMAX/pcmin_revised.f.

341 values occur over the Atlantic in low-latitudes, the Caribbean Sea, and Gulf of Mexico, where a
342 majority of TC genesis takes place.

343 An important consideration is whether the above modifications in the convective
344 parameterization produce changes in the atmospheric mean state and its variability (e.g., seasonal
345 cycle) that are within acceptable ranges. Slingo et al. (1994) and Zhang and McFarlane (1995)
346 found some sensitivity of the tropical mean climate to the parameterized moist convection.
347 Figure 15 shows the differences between each experiment in the mean precipitation for 2005. We
348 plot both the large-scale precipitation and convective precipitation to indentify the fractional
349 precipitation changes. The left panels show the difference between ExpA and ExpC in total
350 precipitation (Fig. 15a), large-scale precipitation (Fig. 15b) and convective precipitation (Fig.
351 15c). The results show that both total and large-scale precipitation increase noticeably over the
352 tropics for ExpA, whereas there is a substantial reduction in convective precipitation. In contrast,
353 for ExpB (the right panels) there is only a very small change in total precipitation over the
354 tropics (Fig. 15d), while the large-scale precipitation over the TC genesis region increases
355 slightly (Fig. 15e) along with a decrease in convective precipitation (Fig. 15f). This fractional
356 precipitation change is due to an increased activity of grid-scale cloud/condensation (i.e., large-
357 scale precipitation) along with a suppression of parameterized deep convection (i.e., convective
358 precipitation) (Reed and Jablonowski 2011; Zhao et al. 2012).

359 The area-averaged difference in total precipitation over the Atlantic basin between ExpB
360 and ExpC (Table 3) is 0.03 mm day^{-1} in 2005 and 0.09 mm day^{-1} in 2006, while for ExpA the
361 precipitation increases with respect to ExpC by 0.5 and 0.6 mm day^{-1} in those two years,
362 respectively. All three experiments overestimate the observed precipitation (left column in Table
363 3; see also Fig. 16a). Since the observationally-based precipitation estimates from the Global

Precipitation Climatology Project (GPCP) version 2.2 (Adler et al. 2003; Huffman et al. 2009) are provided on a relatively coarse grid (2.5° lon.-lat.), we speculate that part of the apparent overestimation by the model might in fact represent an underestimation of the coarser resolution GPCP precipitation. Table 3 indicates that the excessive total precipitation in ExpA makes it a less than ideal model to use even though it has more intense hurricanes. Also, ExpA produces an excessive number of storms during the inactive hurricane year of 2006 (Table 1). In contrast, ExpB seems a better option since it has minimal impact on the total precipitation (amount and spatial distribution), and it has improved 3-dimensional hurricane structures, intensities, and numbers, compared with the control (ExpC).

Figure 16 compares for each experiment the seasonal variation (June through November) of precipitation, SLP, surface temperature and upper-level wind speed over the typical TC genesis region. We see that ExpB tends to remain close to ExpC in all the variables, while ExpA shows a noticeable increase in total precipitation and surface temperature, and decrease in SLP compared to the control run. A comparison with observations indicates that, except for the upper-level wind speed, ExpA tends to have larger biases than either ExpB or the control (ExpC). Overall, our results suggests that a small reduction in the influence of the RAS convective parameterization (ExpB) produces improved North Atlantic TC activity without having a negative impact on the mean climate of the model when run at ¼ degree spatial resolution.

5. Concluding remarks and discussion

This study investigated the sensitivity of the North Atlantic TC activity to changes in parameterized deep convection in the NASA GEOS-5 model run at 0.25 degree latitude/longitude horizontal resolution. The study found that reduction in the influence of the

RAS scheme resulting from an increase in minimum entrainment for parameterized deep convection improves/enhances (compared to the standard control model) the TC activity in terms of numbers, intensity, life cycle, and the 3-dimensional storm structures. Our case studies for the 2005 (very active) and 2006 (very inactive) hurricane seasons revealed that only a modest increase in minimum entrainment (ExpB) was necessary at a quarter-degree resolution to produce TC numbers reasonably close to observations. The strongest hurricane reached a minimum SLP of 940hPa and low-level maximum wind speeds greater than 60m/s. The vertical structure is characterized by a well-defined hurricane eye, an upper-tropospheric warm core value exceeding 10°C, and maximum winds located at low levels within 50km of hurricane center. These magnitudes are comparable to, or improvement over, those of Shen et al. (2006) and Reed and Jablonowski (2011) at similar resolution. Furthermore, we found that a stronger constraint on the parameterized deep convection (i.e., ExpA) produced even stronger hurricanes (with minimum SLP of 935hPa, and a maximum wind speed of 65m/s), but this strong reduction in parameterized convection was not desirable as it produced strong TC activity even in a weak hurricane year (2006) and lead to increased bias in the atmospheric mean state.

Our analysis of the causes of the TC changes suggests that the following processes are at work. First, an increase in the threshold of minimum entrainment causes more entrainment of dry air into the convective plume. This entraining process leads to a reduction in buoyancy, resulting in less favorable conditions for deep convection. This leads to a reduction in condensation heating in the upper-troposphere, resulting in upper-tropospheric cooling. As a result, the upper-troposphere becomes drier and cooler, while the lower-troposphere becomes moister and warmer. This is accompanied by an increase in positive near-surface latent heat flux. This change in the vertical structure of the atmosphere is apparent over the Atlantic basin, easing the condition for

developing atmospheric instability. The greater instability is evidenced by changes in the profile of moist static energy, the vertical gradient of equivalent potential temperature, and the distribution of CAPE. As a consequence to the changes in atmospheric instability there is an increase in a) low level positive vorticity and convergence, b) upward motion, and 3) low-level moisture flux convergence. These changes help the development of explicit-scale convection and subsequent large-scale condensation of wave vapor, and represent a transition of the moist deep convection from the parameterized kind to that occurring at the resolved scales. This is reflected by a decrease in convective precipitation contributed by parameterized convection and an increase in large-scale precipitation. The above interpretation is supported by the changes in the GPI (Emanuel and Nolan 2004; Murakami et al. 2011) showing (for ExpB) an enhancement in the TC activity over the Atlantic, with more and stronger TCs than the control run (e.g., category 4 hurricanes were produced, whereas the control never produced hurricanes stronger than category 3).

The explicit-scale moist convection favored by atmospheric instability appears to compensate for the upper-tropospheric cooling and drying produced by the reduction in parameterized deep convection, with the atmosphere acting to maintain thermal equilibrium in the upper-troposphere. This likely explains why, at least for the experiment with only a modest change in the threshold of minimum entrainment (ExpB), the total precipitation remains close to those of the control.

Due to the limited number of cases investigated here, it is premature to say that ExpB truly represents an optimal setting for the reliable simulation of TCs at this resolution. Nevertheless, the current set of experiments are encouraging in that they demonstrate how years with widely differing TC activity (2005 and 2006) can be reproduced by global climate model with a rather

433 minor change to the convective parameterization, and that this can be done without degrading the
434 mean state.

435 This article suggests that quarter-degree horizontal resolution may be the minimum
436 resolution necessary for achieving realistic TC simulations via modifications to the
437 parameterized convective process (Reed and Jablonowski 2011), while still maintaining a
438 realistic mean state. This conclusion is based in part on other experiments we carried out at half
439 and one-third degree resolution (not shown), in which realistic TC numbers were difficult to
440 achieve without modifying the threshold values for TC detection. Of course the results at ¼
441 degree resolution still have several limitations. Key among them is the inability to produce the
442 most intense (category 5) hurricanes. It appears that even at substantially finer than a quarter-
443 degree resolution, fine scale hurricane structure can be improved through the modification of the
444 convective parameterization. For example, Putman and Suarez (2011) concluded from the
445 analysis of GEOS-5 forecasts run at 7-km horizontal resolution, that intense precipitation was
446 better formed within the hurricane eye-wall and surrounding rain bands with a reduction in the
447 influence of the RAS convective parameterization, compared to a control in which RAS was not
448 modifed. As such it appears that, even at considerably higher resolution than considered here,
449 improvements in the simulation of TC activity can still benefit from a proper modification of the
450 convective parameterization.

451

452 **References**

453 Adler, R. F., and Coauthors, 2003: The version 2 Global Precipitation Climatology Project
454 (GPCP) monthly precipitation analysis (1979-present). *J. Hydrometeor*., **4**, 1147-1167.

455 Arakawa, A., and W. H. Schubert, 1974: Interaction of cumulus cloud ensemble with the large-
456 scale environment. Part I. *J. Atmos. Sci*., **31**, 671-701.

457 Atlas, R., O. Reale, B.-W. Shen, S.-J. Lin, J.-D. Chern, W. Putmann, T. Lee, K.-S. Yeh, M.
458 Bosilovich, and J. Radakovich, 2005: Hurricane forecasting with the high-resolution NASA
459 finite volume general circulation model. *Geophys. Res. Lett*., **32**, L03807,
460 doi:10.1029/2004GL021513.

461 Bacmeister, J. T., and G. L. Stephens, 2011: Spatial statistics of likely convective clouds in
462 CloudSat data. *J. Geophys. Res*., **116**, D04104, doi:10.1029/2010JD014444.

463 Benjamin, M. S., C. Piani, W. Ingram, D. Stone, and M. Allen, 2008: Towards constraining
464 climate sensitivity by linear analysis of feedback patterns in thousands of perturbed physics
465 GCM simulations. *Clim. Dyn*., **30**, 175-190.

466 Bister, M., and K. A. Emanuel, 1998: Dissipative heating and hurricane activity. *Meteor. Atmos.*
467 *Phys*., **52**, 233-240.

468 Caron, L.-P., C. G. Jones, and K. Winger, 2011: Impact of resolution and downscaling technique
469 in simulating recent Atlantic tropical cyclone activity. *Clim. Dyn*., **37**, 869-892.

470 Daloz, A.-S., F. Chauvin, K. Walsh, S. Lavender, D. Abbs, and F. Roux, 2012: The ability of
471 GCMs to simulate tropical cyclones and their precursors over the North Atlantic main
472 development region. *Clim. Dyn.,* **39**, 1559-1576.

473 Emanuel, K. A., 1995: Sensitivity of tropical cyclones to surface exchange coefficients and a
474 revised steady-state model incorporating eye dynamics. *J. Atmos. Sci*., **52**, 3969-3976.
475 Emanuel, K. A., and D. S. Nolan, 2004: Tropical cyclone activity and global climate.
476 Proceedings, *The 26th Conference on Hurricanes and Tropical Meteorology*, Miami, FL,
477 Amer. Meteor. Sci., 240-241.
478 Emanuel, K. A., R. Sundararajan, and J. Williams, 2008: Hurricanes and global warming:
479 Results from downscaling IPCC AR4 simulations. *Bull. Amer. Meteor. Soc*., **89**, 347-367.
480 Emanuel, K. A., 2013: Downscaling CMIP5 climate models shows increased tropical cyclone
481 activity over the 21st century. *Proc. Nat. Acad. Sci*., **110**, doi: 10.1073/pnas.1301293110.
482 Frank, W. M., 1977: The structure and energetic of the tropical cyclone. I. Storm structure. *Mon.*
483 *Wea. Rev*., **105**, 1119-1135.
484 Gent, P. R., and co-authors, 2011: The Community Climate System Model Version 4. *J. Climate*,
485 **24**, 4973-4991.
486 Held, I. M., M. Zhao, and B. Wyman, 2007: Dynamic radiative–convective equilibria using
487 GCM column physics. *J. Atmos. Sci.*, **64**, 228–238.
488 Huffman, G. J., R. F. Adler, D. T. Bolvin, and G. Gu, 2009: Improving the Global Precipitation
489 record: GPCP version 2.1. *Geophys. Res. Lett*., **36**, L17808, doi:10.1029/2009GL040000.
490 Kang, S. M., I. M. Held, D. M. W. Frierson, and M. Zhao, 2008: The response of the ITCZ to
491 extratropical thermal forcing: Idealized slab-ocean experiments with a GCM. *J. Climate*, **21**,
492 3521–3532.
493 Knapp, K. R., M. C. Kruk, D. H. Levinson, H. J. Diamond, and C. J. Neumann, 2010: The
494 international best track archive for climate stewardship (IBTrACS) : Unifying tropical

cyclone best track data. *Bull. Amer. Meteor. Soc*., **91**, 363-376, doi:10.1175/2009BAMS2755.

Knutson, T. R., and R. E. Tuleya, 2004: Impact of CO2-induced warming on simulated hurricane intensity and precipitation: Sensitivity to the choice of climate model and convective parameterization. *J. Climate*, **17**, 3477–3495.

Knutson, T. R., J. J. Sirutis, S. T. Garner, I. M. Held, and R. E. Tuleya, 2007: Simulation of the recent multidecadal increase of Atlantic hurricane activity using an 18-km-grid regional model. B*ull. Amer. Meteor. Soc.*, **88**, 1549–1565.

LaRow, T., Y.-K. Lim, D. Shin, E. Chassignet, and S. Cocke, 2008: Atlantic basin seasonal hurricane simulations. *J. Climate*, **21**, 3191-3206.

Lee, M.-I., I.-S. Kang, and B. E. Mapes, 2003: Impacts of cumulus convection parameterization on aqua-planet AGCM simulations of tropical intraseasonal variabilility. *J. Meteor. Soc. Japan*, **81**, 963-992.

Lin, J.-L., M.-I. Lee, D. Kim, I.-S. Kang, and D. M. W. Frierson, 2008: Impacts of convective parameterization and moisture convective trigger on AGCM-simulated convectively coupled equatorial waves. *J. Climate*, **21**, 883-909.

Ma, L.-M. and Z.-M. Tan, 2009: Improving the behavior of the cumulus parameterization for tropical cyclone prediction: Convection trigger. *Atmos. Res*., **92**, 190-211.

Manabe, S., 1969: Climate and the ocean circulation: I. The atmospheric circulation and the hydrology of the Earth's surface. *Mon. Wea. Rev*., **97**, 739-774.

Molod, A., L. Takacs, M. Suarez, J. Bacmeister, I.-S. Song, and A. Eichmann, 2012: The GEOS-5 Atmospheric General Circulation Model: Mean Climate and Development from MERRA

517 to Fortuna. *NASA Technical Report Series on Global Modeling and Data Assimilation,*
518 *NASA TM—2012-104606*, **28**, 117 pp.
519 Moorthi, S., and M. J. Suarez, 1992: Relaxed Arakawa-Schubert: A parameterization of moist
520 convection for general circulation models. *Mon. Wea. Rev*., **120**, 978-1002.
521 Murakami, H., B. Wang, and A. Kitoh, 2011: Future change of western north Pacific typhoons:
522 Projections by a 20-km-mesh global atmospheric model. *J. Climate*, **24**, 1154-1169.
523 Noda, A. T., K. Oouchi, M. Satoh, and H. Tomita, 2012: Quantitative assessment of diurnal
524 variation of tropical convection simulated by a global nonhydrostatic model without
525 cumulus parameterization. *J. Climate*, **25**, 5119-5134.
526 Oouchi, K., J. Yoshimura, H. Yoshimura, R. Mizuta, S. Kusunoki, and A. Noda, 2006: Tropical
527 cyclone climatology in a global-warming climate as simulated in a 20-km mesh global
528 atmospheric model: Frequency and wind intensity analysis. *J. Meteor. Soc. Japan*, **84**, 259–
529 276.
530 Putman, W. M., and M. Suarez, 2011: Cloud-system resolving simulations with the NASA
531 Goddard Earth Observing System global atmospheric model (GEOS-5). *Geophys. Res. Lett*.,
532 **38**, L16809, doi:10.1029/2011GL048438.
533 Rayner, N. A., and Coauthors, 2003: Global analyses of sea surface temperature, sea ice, and
534 night time air temperature since the late nineteenth century. *J. Geophys. Res*., **108,** (D14),
535 4407, doi:10.1029/2002JD002670.
536 Rienecker M. M. and Coauthors, 2008: The GEOS-5 data assimilation system – documentation
537 of versions 5.0.1 and 5.1.0, and 5.2.0. In: NASA technical report series on global modeling
538 and assimilation, NASA/TM-2008-104606, **27**, 92pp.

539 Rienecker, M.M., and Coauthors, 2011: MERRA - NASA's Modern-Era Retrospective Analysis
540 for Research and Applications. *J. Climate*, **24**, 3624-3648. doi: 10.1175/JCLI-D-11-00015.1.
541 Reed, K. A., and C. Jablonowski, 2011: Impact of physical parameterizations on idealized
542 tropical cyclones in the Community Atmosphere Model. *Geophys. Res. Lett*., **38**, L04805,
543 doi:10.1029/2010GL046297.
544 Shaevitz, D. A., and Coauthors, 2014: Characteristics of tropical cyclones in high-resolution
545 models in the present climate. Submitted to *J. Climate*,
546 Shen, B.-W., R. Atlas, O. Reale, S.-J. Lin, J.-D. Chen, J. Chang, C. Henze, and J.-L. Li, 2006:
547 Hurricane forecasts with a global mesoscale-resolving model: Preliminary results with
548 Hurricane Katrina (2005). *Geophys. Res. Lett*., **33**, L13813, doi:10.1029/2006GL026143.
549 Simpson, J. , and V. Wiggert, 1969: Models of precipitating cumulus towers, *Mon. Wea. Rev.*, **97**,
550 471-480.
551 Slingo, J., and Coauthors, 1994: Mean climate and transience in the tropics of the UGAMP
552 GCM: Sensitivity to convective parameterization. *Quart. J. Roy. Meteor. Soc*., **120**, 881-922.
553 Smith, R. K., 2000: The role of cumulus convection in hurricanes and its representation in
554 hurricane models. *Rev. Geophys*., **38**, 465-489.
555 Stan, C., 2012: Is cumulus convection the concertmaster of tropical cyclone activity in the
556 Atlantic? *Geophys. Res. Lett*., **39**, doi: 10.1029/2012GL053449.
557 Stephens, G., and Coauthors, 2002: The CloudSat mission and the A-Train. Bull. Amer. Meteor.
558 Soc., 83, 1771-1790.
559 Strachan, J., P.-L. Vidale, K. Hodges, M. Roberts, and M.-E. Demory, 2013: Investigating global
560 tropical cyclone activity with a hierarchy of AGCMs: The role of model resolution. *J.*
561 *Climate*, **26**, 133–152.

562 Tiedke, M., 1993: Representation of clouds in large-scale models. *Mon. Wea. Rev*., **121**, 3040-
563 3061.
564 Tokioka, T., K. Yamazaki, A. Kitoh, and T. Ose, 1988: The equatorial 30–60 day oscillation and
565 the Arakawa-Schubert penetrative cumulus parameterization, *J. Meteorol. Soc. Japan*., **66**,
566 883–901.
567 Vitart, F., J. L. Anderson, J. Sirutis, and R. E. Tuleya, 2001: Sensitivity of tropical storms
568 simulated by a general circulation model to changes in cumulus parameterization. *Quart. J.*
569 *Royal Meteor. Soc*., **127**, 25-51.
570 Vitart, F., D. Anderson, and T. Stockdale, 2003: Seasonal forecasting of tropical cyclone landfall
571 over Mozambique. *J. Climate*, **16**, 3932-3945.
572 Walsh, K. J. E., M. Fiorino, C. W. Landsea, and K. L. McInnes, 2007: Objectively determined
573 resolution-dependent threshold criteria for the detection of tropical cyclones in climate
574 models and reanalyses. *J. Climate,* **20,** 2307–2314.
575 Walsh, K., S. Lavender, E. Scoccimarro, and H. Murakami, 2013: Resolution dependence of
576 tropical cyclone formation in CMIP3 and finer resolution models. *Clim. Dyn.*, **40**, 585-599.
577 Wang, Z., 2014: Role of cumulus congestus in tropical cyclone formation in a high-resolution
578 numerical model simulation. *J. Atmos. Sci*., early online release.
579 Zhang, G. J., and N. A. McFarlane, 1995: Sensitivity of climate simulations to the
580 parameterization of cumulus convection in the Canadian climate centre general circulation
581 model. *Atmosphere-Ocean*, **33(3)**, 407-446.
582 Zhao, M., I. M. Held, S.-J. Lin, and G. A. Vecchi, 2009: Simulations of global hurricane
583 climatology, interannual variability and response to global warming using a 50-km
584 resolution GCM. *J. Climate*, **22**, 6653-6678.

585 Zhao, M., I. M. Held, and S.-J. Lin, 2012: Some counter-intuitive dependencies of tropical
586 cyclone frequency on parameters in a GCM. *J. Atmos. Sci*., **69**, 2272-2283.

587

588 **Table 1** The number of TCs (middle and bottom row) detected for each year and experiment.
589 Rightmost column represents the observed TC numbers archived at International Best Track
590 Archive for Climate Stewardship (IBTrACS) (Knapp et al. 2010). The values in parenthesis in
591 the middle and bottom row are the number of hurricanes.

	ExpA	ExpB	ExpC (control run)	Observation
2005	36 (24)	25 (15)	18 (8)	29 (15)
2006	27 (21)	13 (8)	8 (6)	10 (5)

592

593

Table 2. List of the threshold values for detecting the TC using the detection/tracking algorithm based on Vitart et al. (2003)

Variables	local relative vorticity maximum (850hPa)	warm core temperature maximum	minimum sea level pressure (SLP)	minimum lower-level wind speed	minimum duration
Criteria	1.0×10^{-4} s^{-1}	6K, Distance between the TC center and the center of the warm core must not exceed 2° lon.&lat.	Minimum SLP defines the TC center and must exist within 2°×2° radius of the vorticity maximum	17m s^{-1}	4 days

602

603 **Table 3**. Difference in total precipitation averaged over the North Atlantic basin that covers
604 90°W-0°E and 0°N-50°N. Difference between ExpA and control run is shown in the middle
605 column whereas the difference between ExpB and control run in the right column. The second
606 and the third row represent the result for the year 2005 and 2006, respectively. Observed
607 precipitation on the left column is obtained from the Global Precipitation Climatology Project
608 (GPCP) dataset, which is 2.5 lon.-lat. gridded.

	ExpA minus ExpC	ExpB minus ExpC
2005 (Obs.=3.62)	4.89-4.40=0.49	4.43-4.40=0.03
2006 (Obs.=3.57)	5.02-4.42=0.60	4.51-4.42=0.09

609

610

611

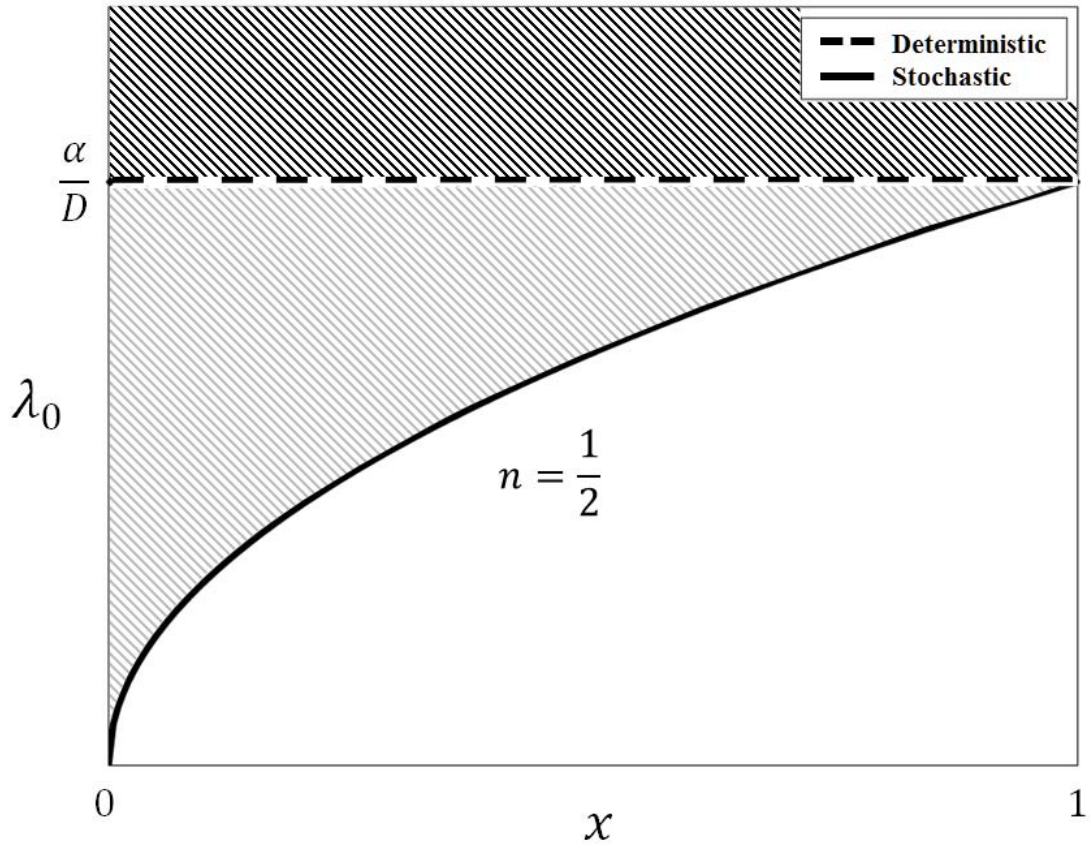

612

613

614 Figure 1 Profile of λ_0 as a function of x in equation (1) with n=1/2 (solid curve). A straight
615 dashed line represents the deterministic $\lambda_0=\alpha/D$, which applies the Tokioka constraint identically
616 at every time step. The entrainment rate of convective plumes need to be higher than λ_0, which
617 range is represented with the black hachured area for the deterministic method. The entrainment
618 rate allowed for the stochastic method is represented with both the black and grey hachured areas.

619

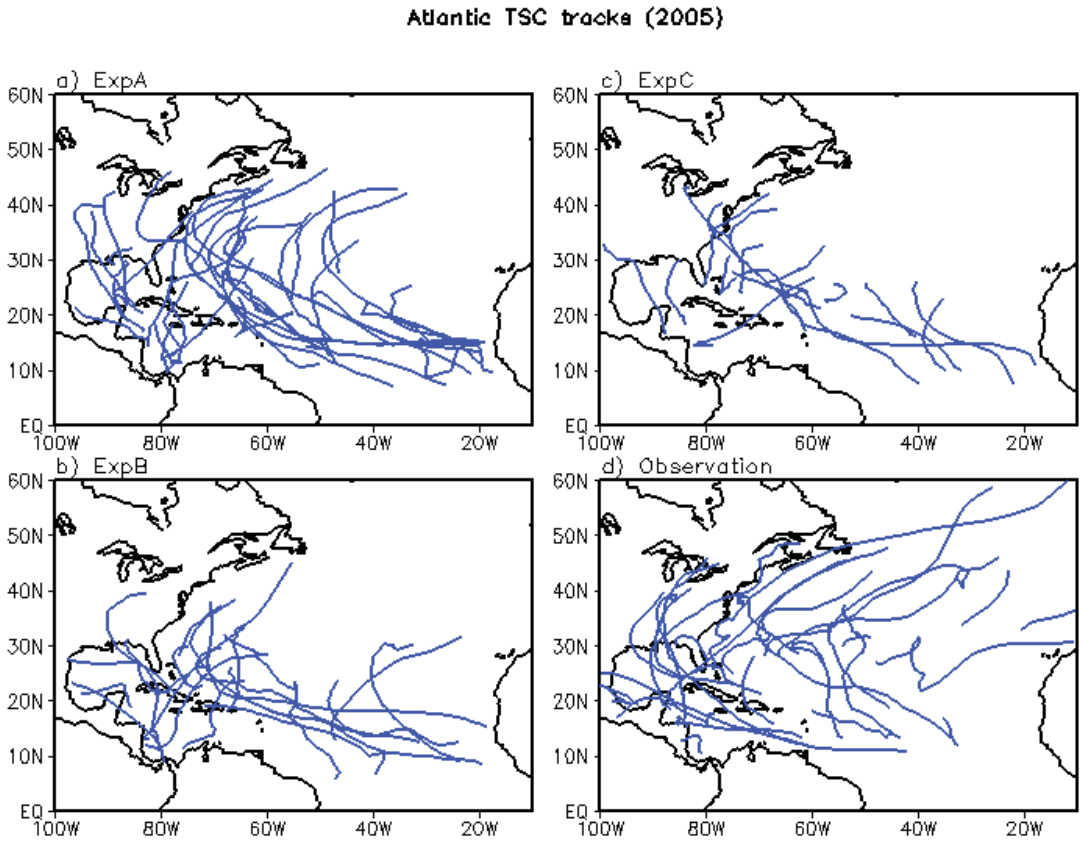

620

621

622 Figure 2. TC tracks for 2005 for a) ExpA, b) ExpB, c) ExpC and d) Observations.

623

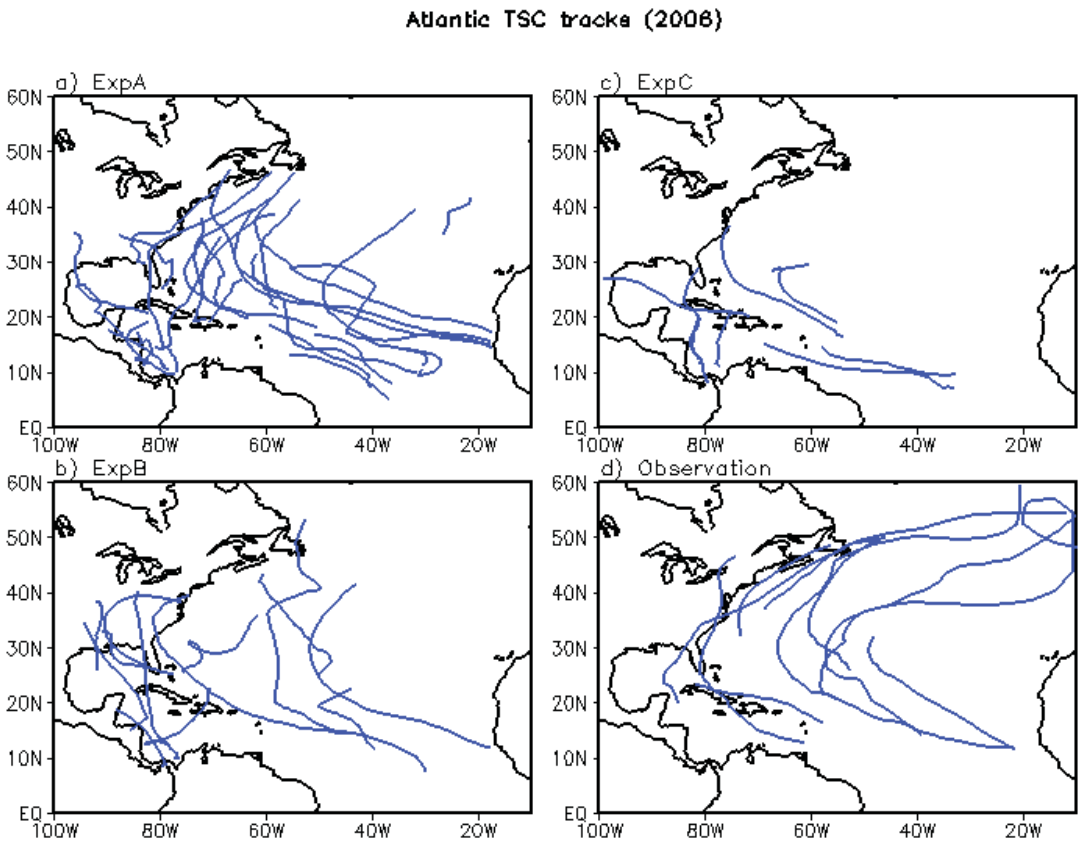

624

625

626 Figure 3. Same as Figure 2, but for 2006.

627

628

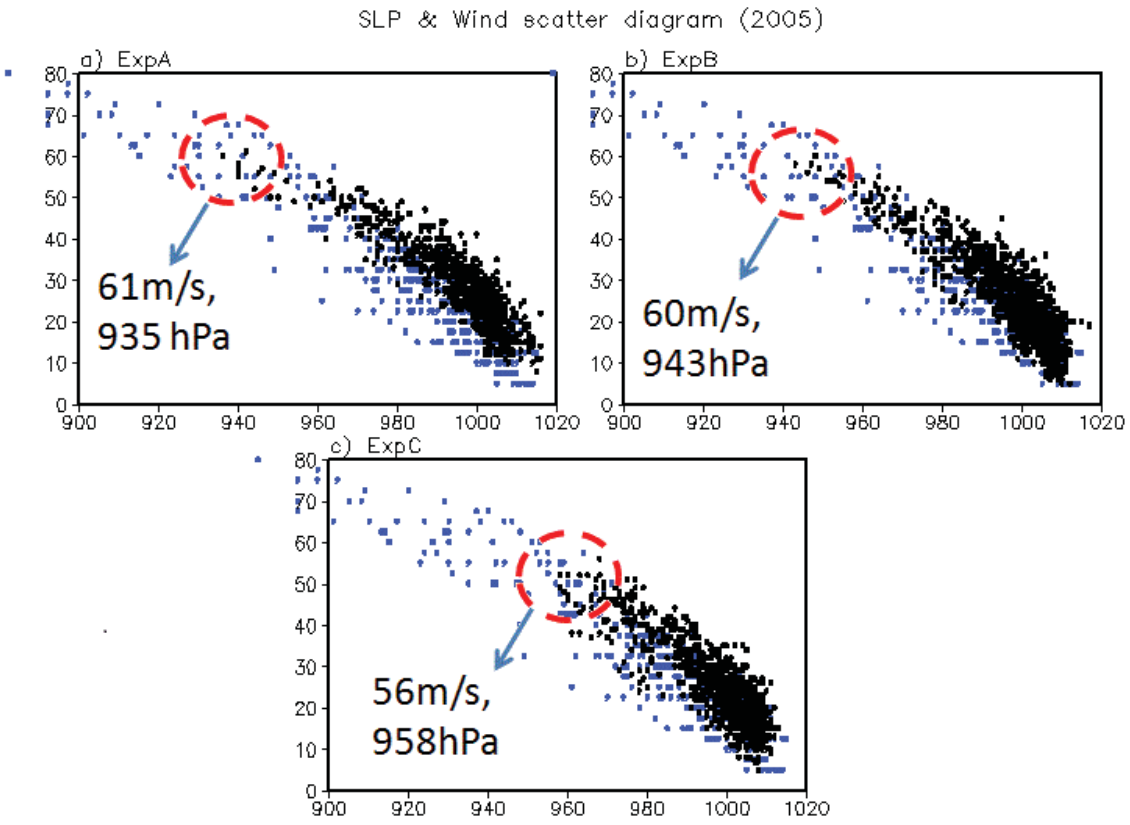

629

630

631 Figure 4. Scatter distribution of sea level pressure (SLP) and lower-level wind speed of TCs in
632 2005 for a) ExpA, b) ExpB and c) ExpC.

633

634

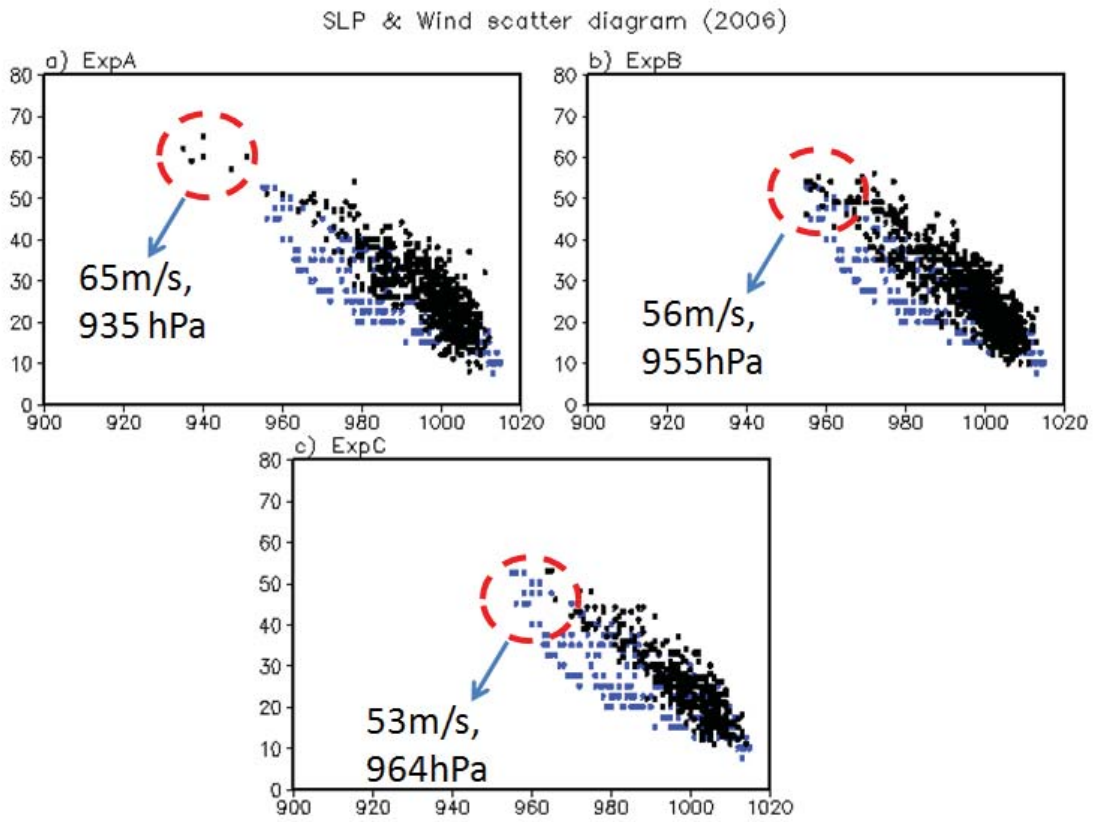

635

636

637 Figure 5. Same as Figure 4 but for 2006.

638

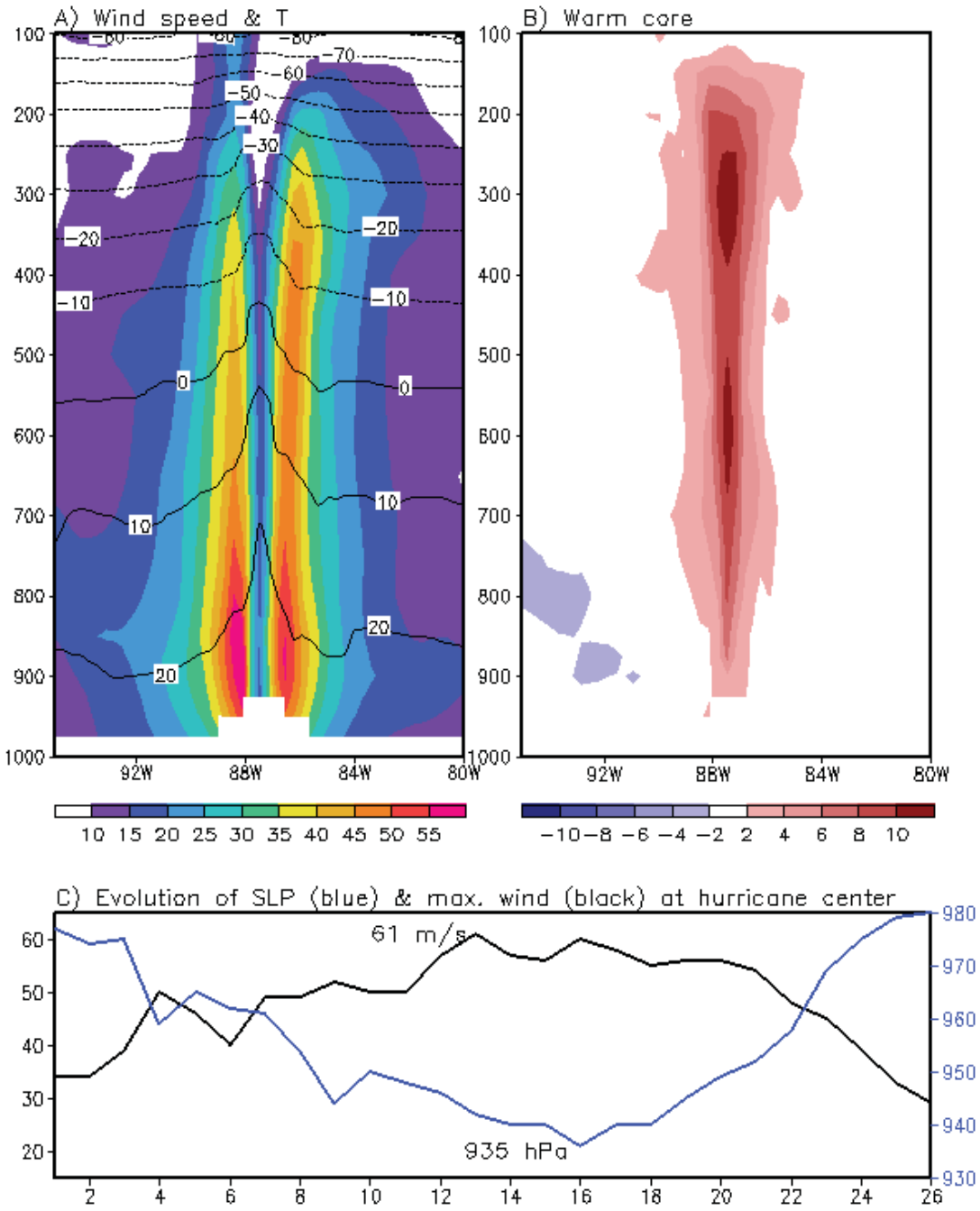

Figure 6. a) and b): Longitude-height cross-section of the strongest hurricane in 2005 simulated by ExpA. Shaded and contoured in a) is wind speed and temperature, respectively, and b) represents warm core computed as temperature deviation from zonal mean over 40° longitudes with a hurricane core centered. Black line on the bottom panel denotes the time evolution of the

maximum wind speed at the lower-level (850-950hPa) of hurricane center whereas blue line the minimum SLP.

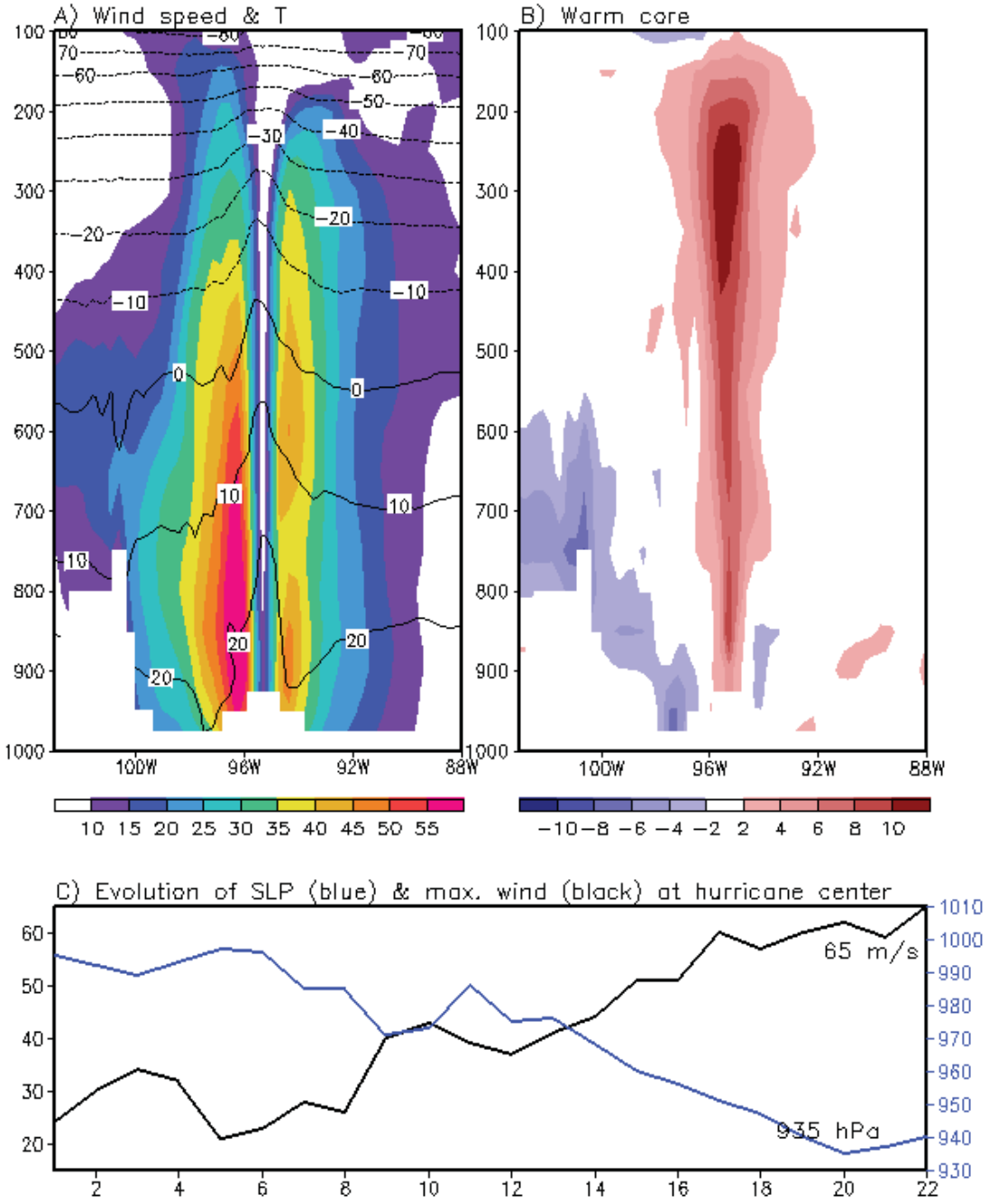

Figure 6: (Continued) Same as the figure on the previous page but for 2006.

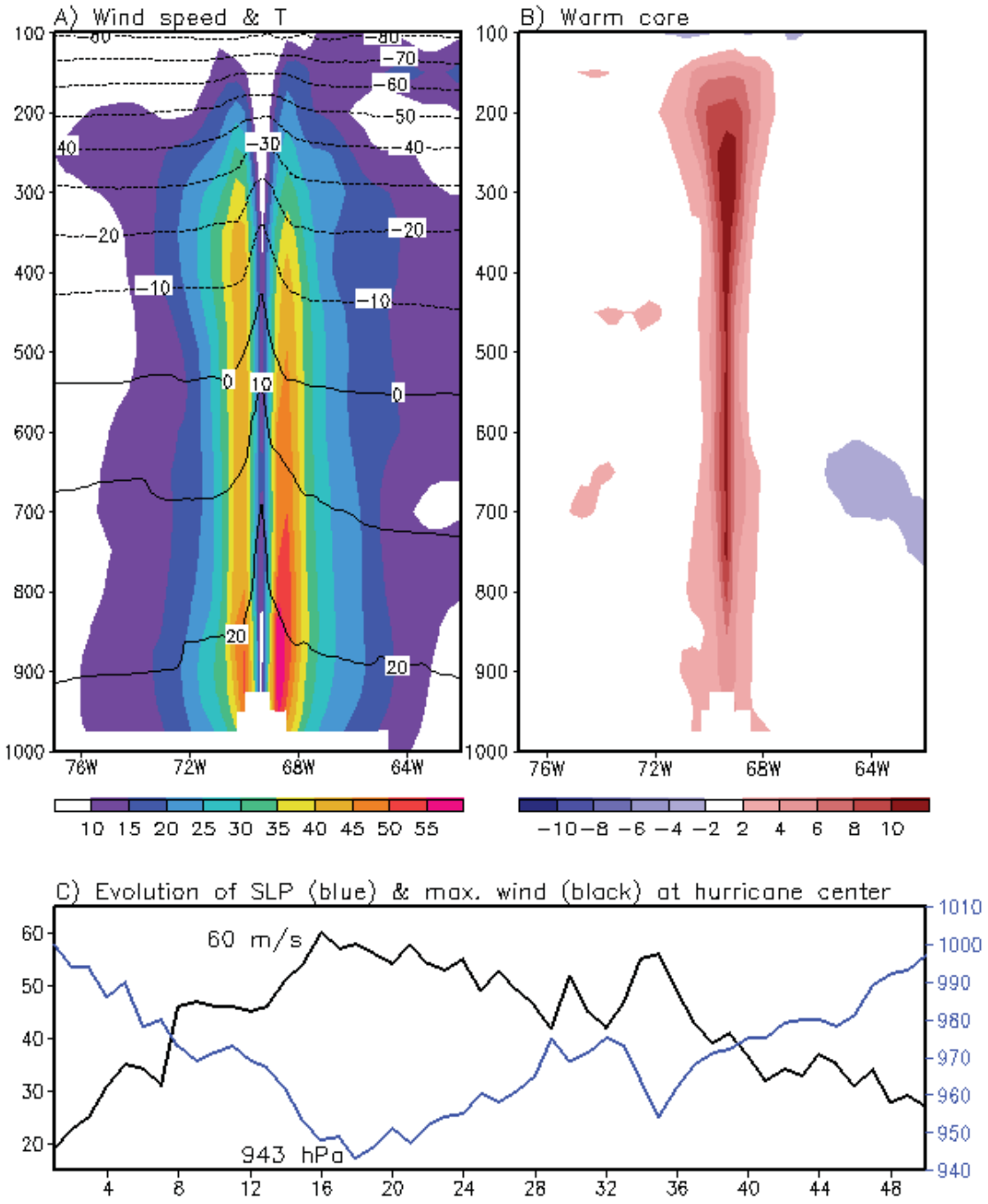

Figure 7. Same as Figure 6 but for ExpB

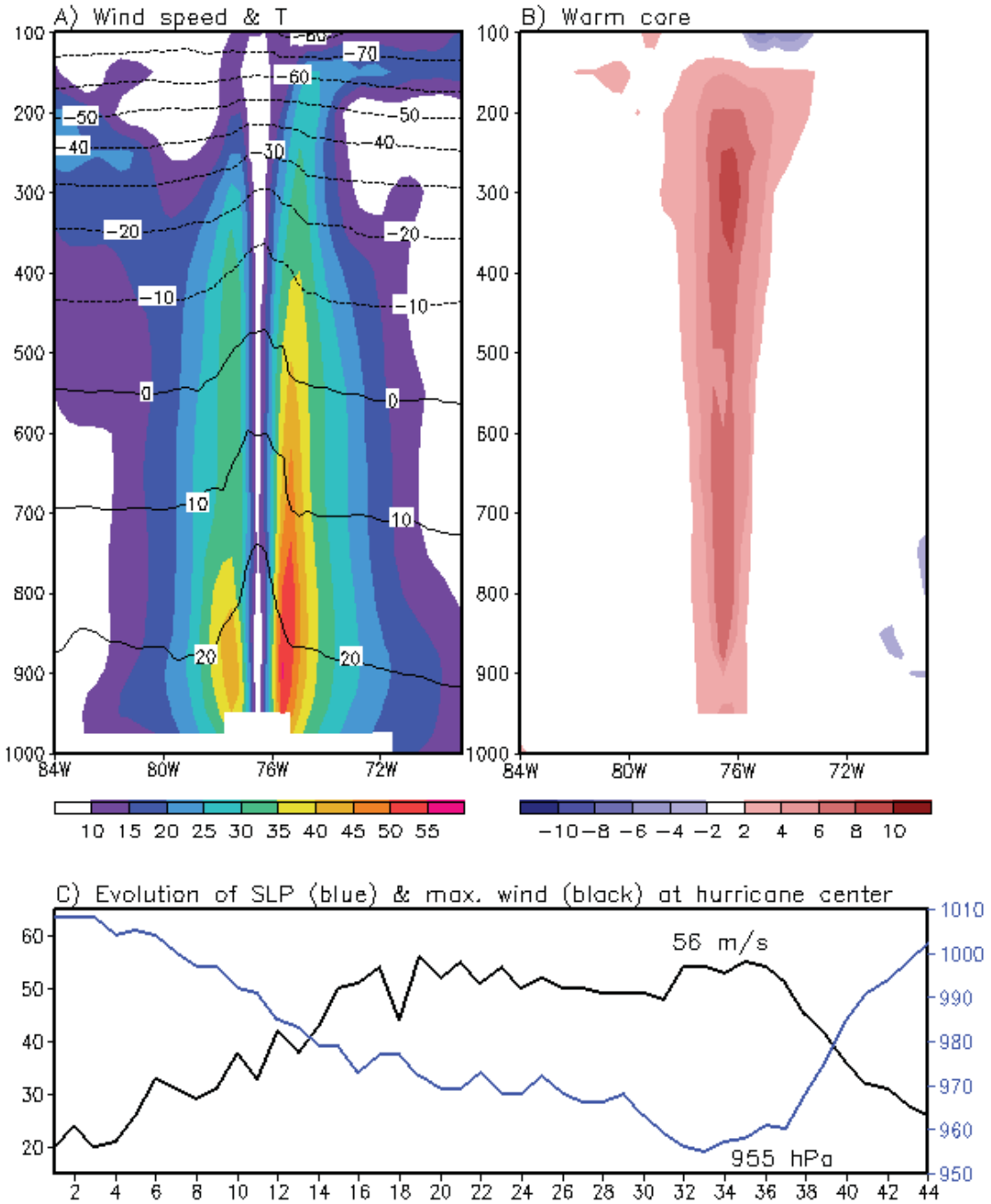

Figure 7: (Continued) Same as the figure on the previous page but for 2006.

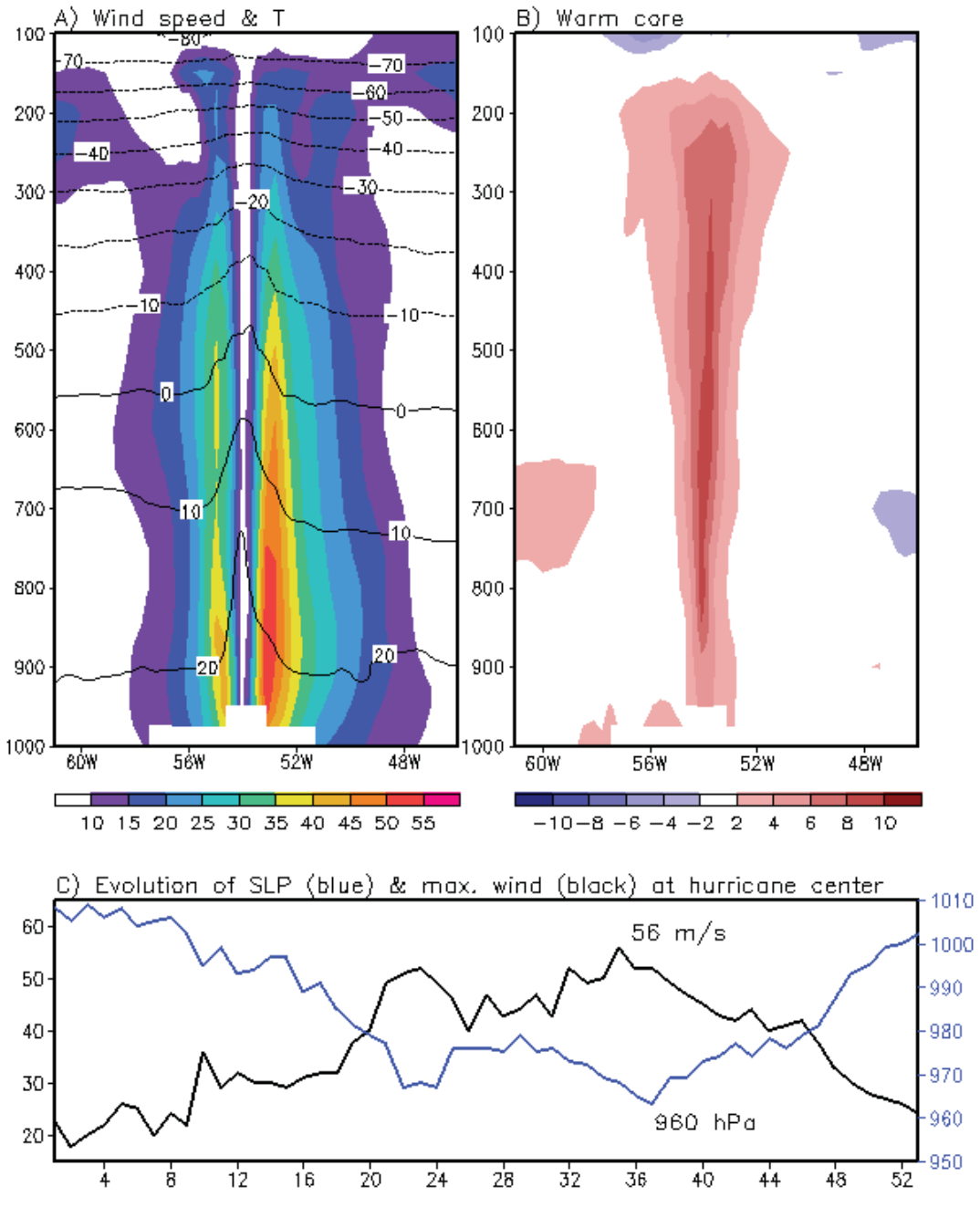

Figure 8. Same as Figure 6 but for ExpC.

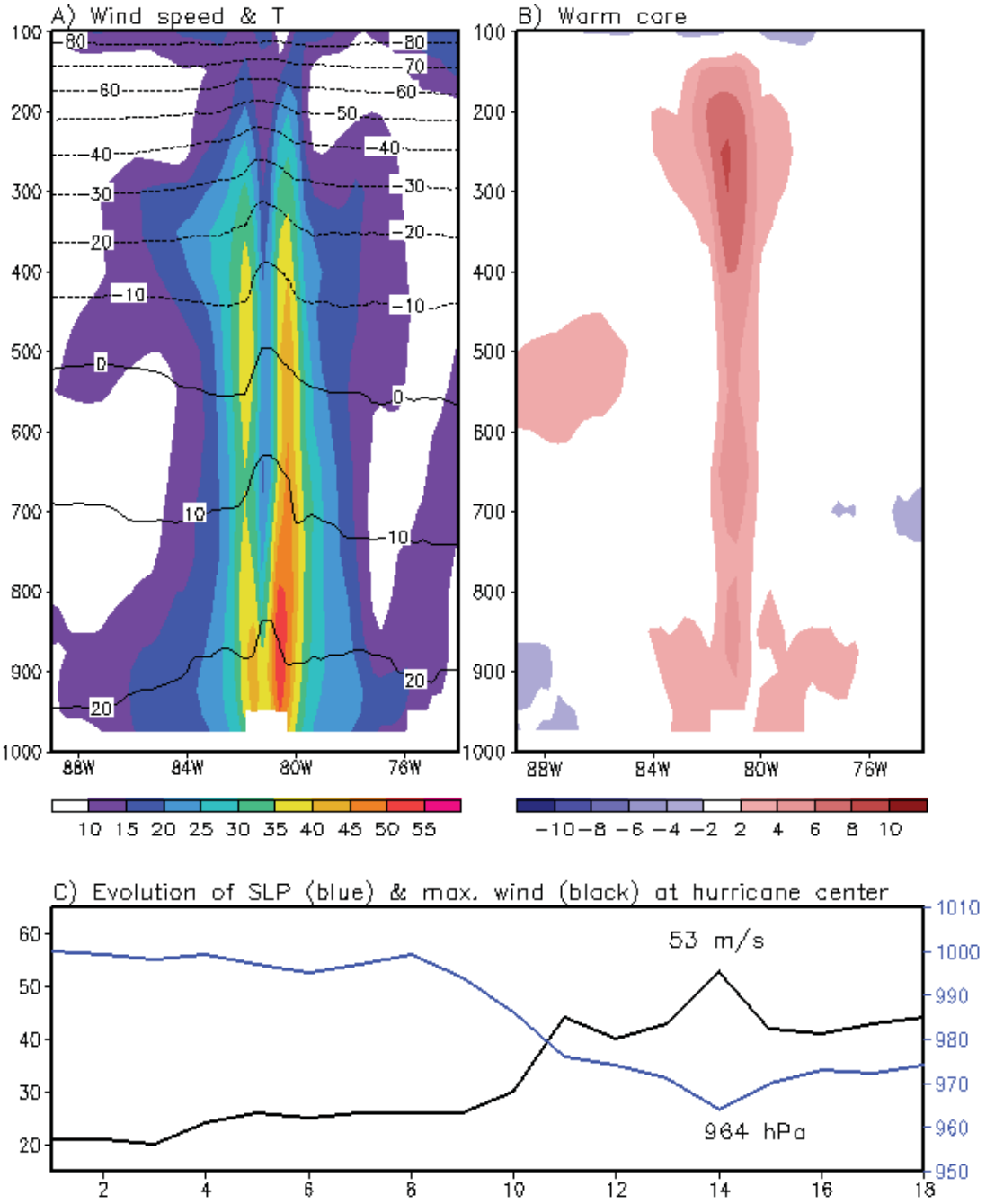

Figure 8: (Continued) Same as the figure on the previous page but for 2006.

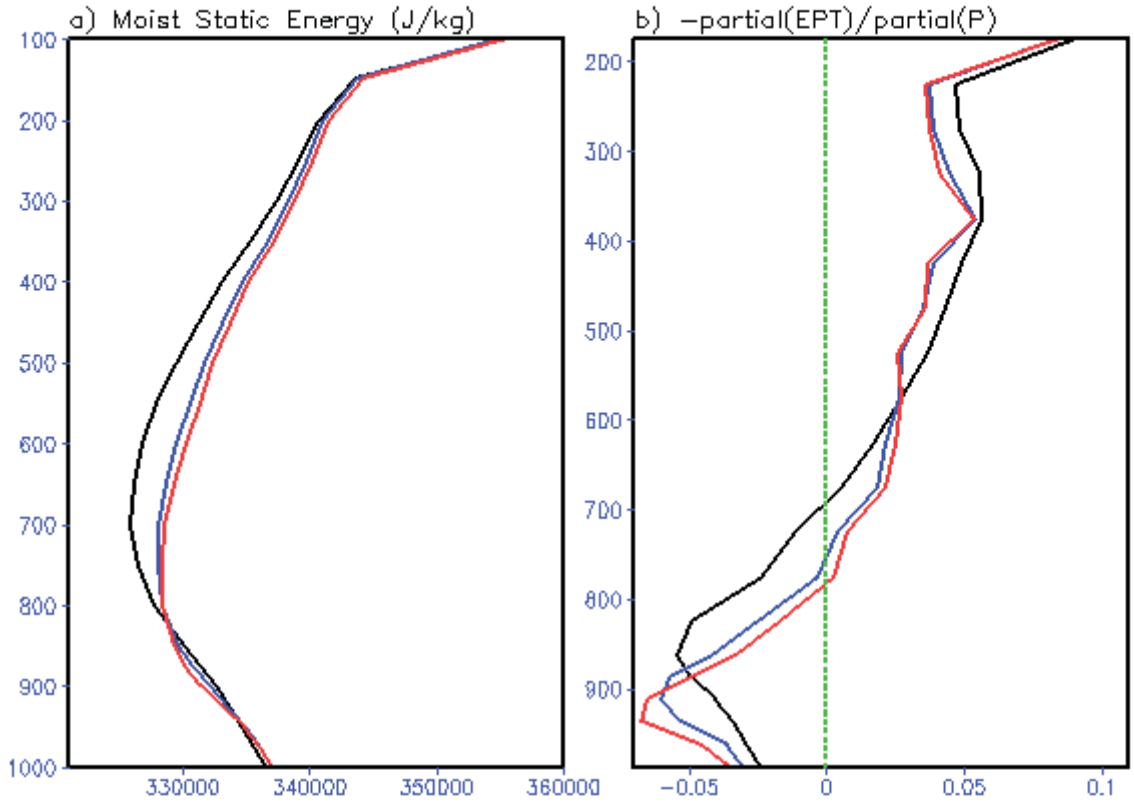

Figure 9. Vertical profile of area-averaged a) moist static energy (J/Kg) and b) vertical gradient of equivalent potential temperature ($-\frac{\partial \theta_e}{\partial p}$) from ExpA (black), ExpB (blue) and ExpC (red) experiments for 2005. Geographical domain for area-averaging covers the typical TC genesis region over the Atlantic that spans 60°W-15°W, 5°N-20°N.

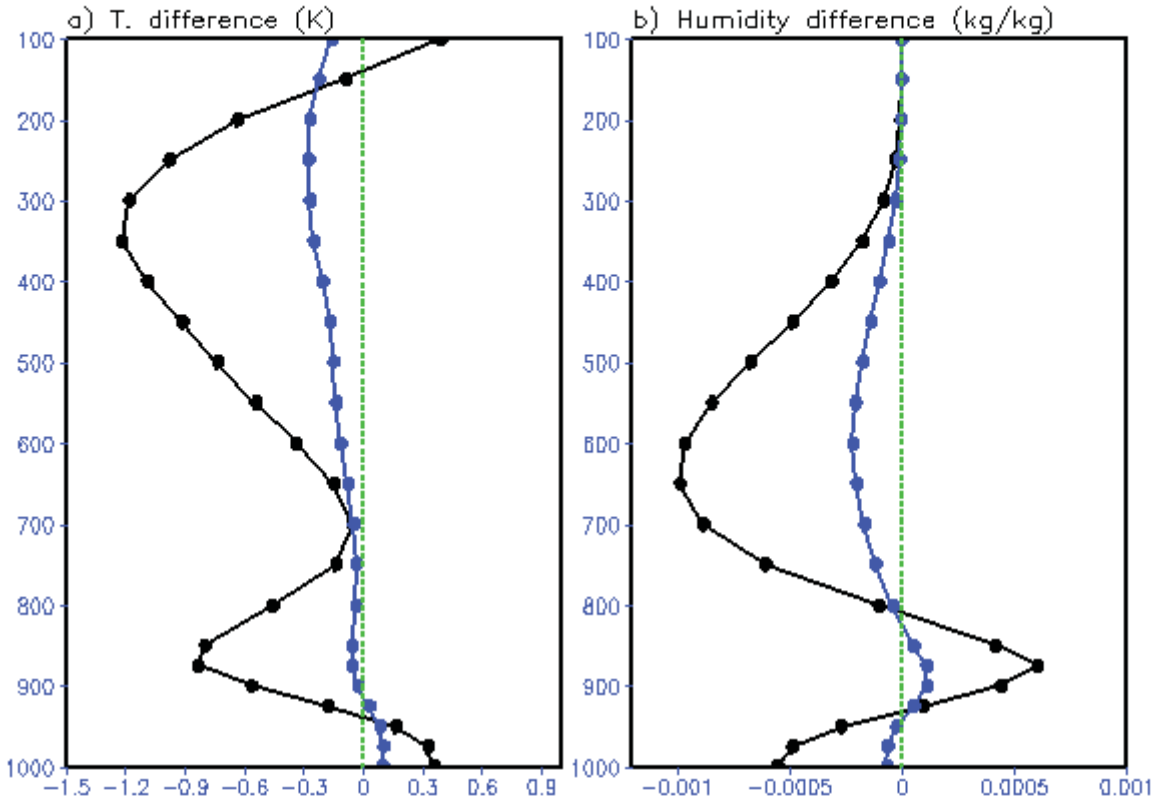

Figure 10. Left: Vertical profile of area-averaged difference in a) temperature and b) specific humidity for 2005. Black curve denotes difference between ExpA and ExpC (ExpA minus ExpC) while the blue curve denotes difference between ExpB and ExpC (ExpB minus ExpC). Geographical domain for area-averaging covers the typical TC genesis region over the Atlantic that spans 60°W-15°W, 5°N-20°N.

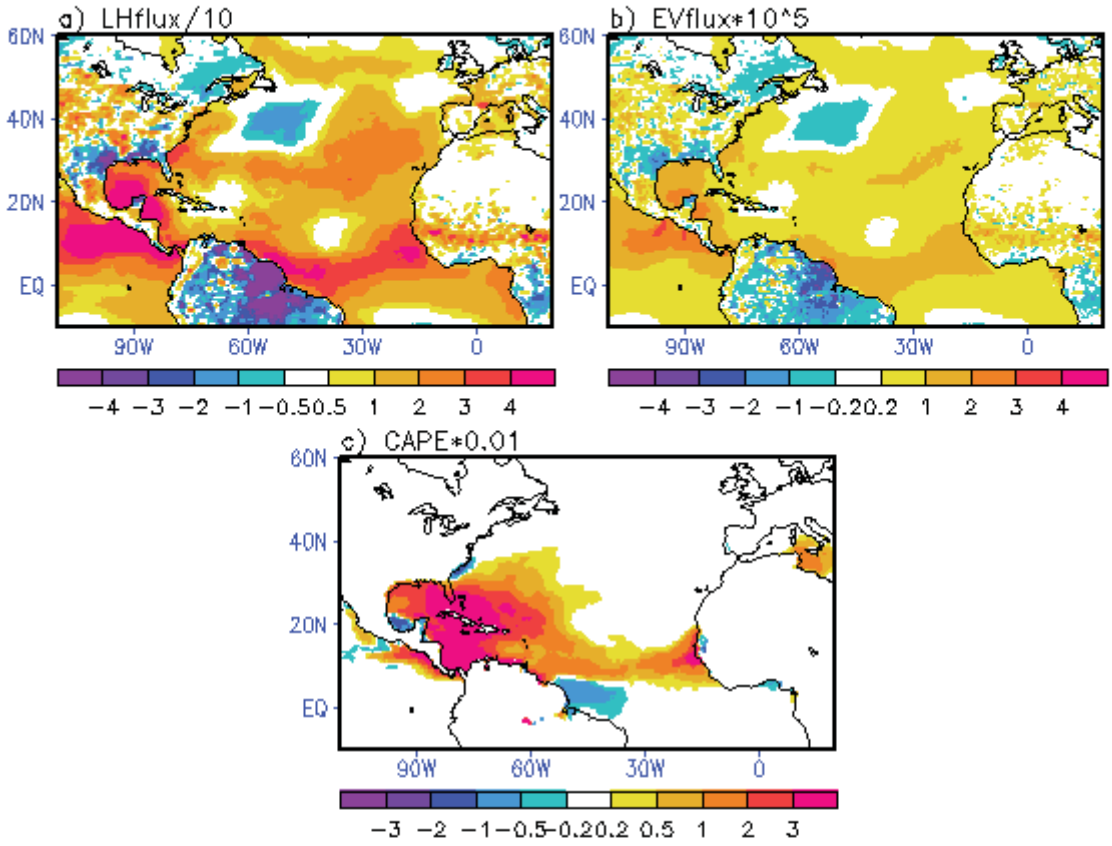

Figure 11. Difference in a) surface latent heat flux, b) evaporative flux, and c) convective available potential energy between ExpA and ExpC (ExpA minus ExpC) during hurricane season (June through November) of 2005.

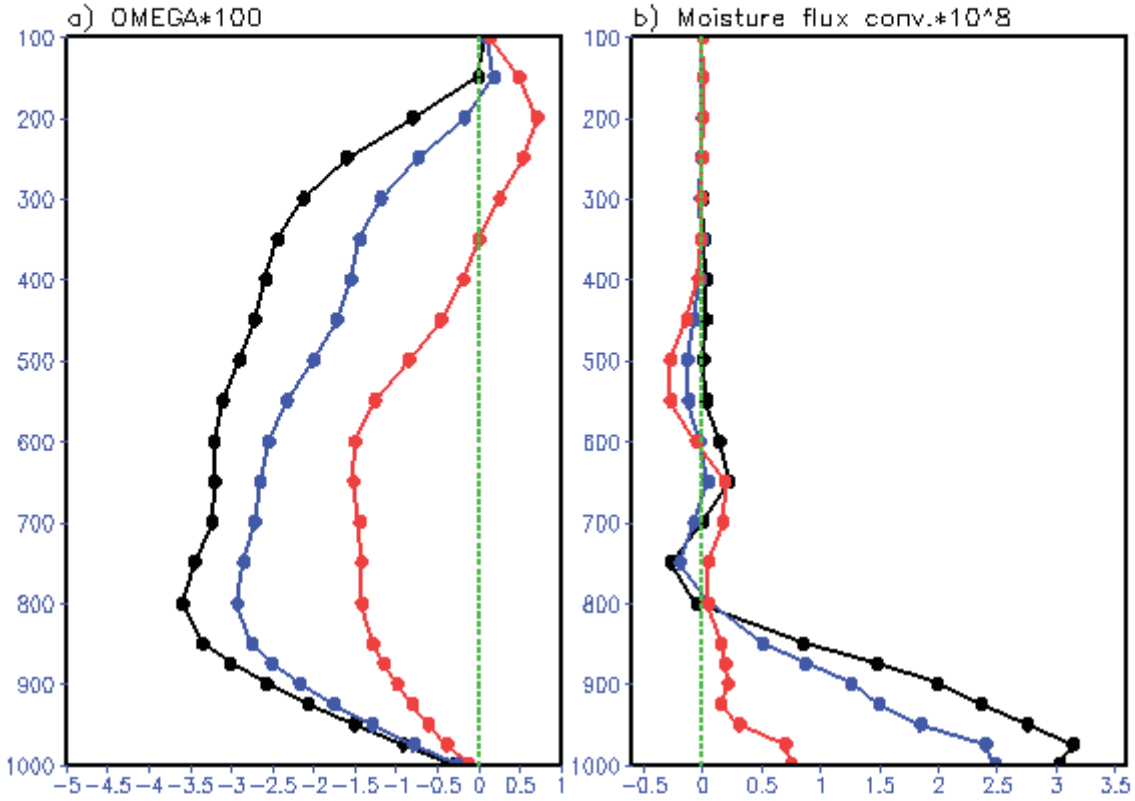

Figure 12. The vertical profile of area-averaged a) omega velocity and b) moisture flux convergence for the hurricane season (June through November) of 2005. The geographical domain for area-averaging covers the typical TC genesis region over the Atlantic that spans 60°W-15°W, 5°N-20°N. Black, blue and red curves denote results for ExpA, ExpB and ExpC, respectively.

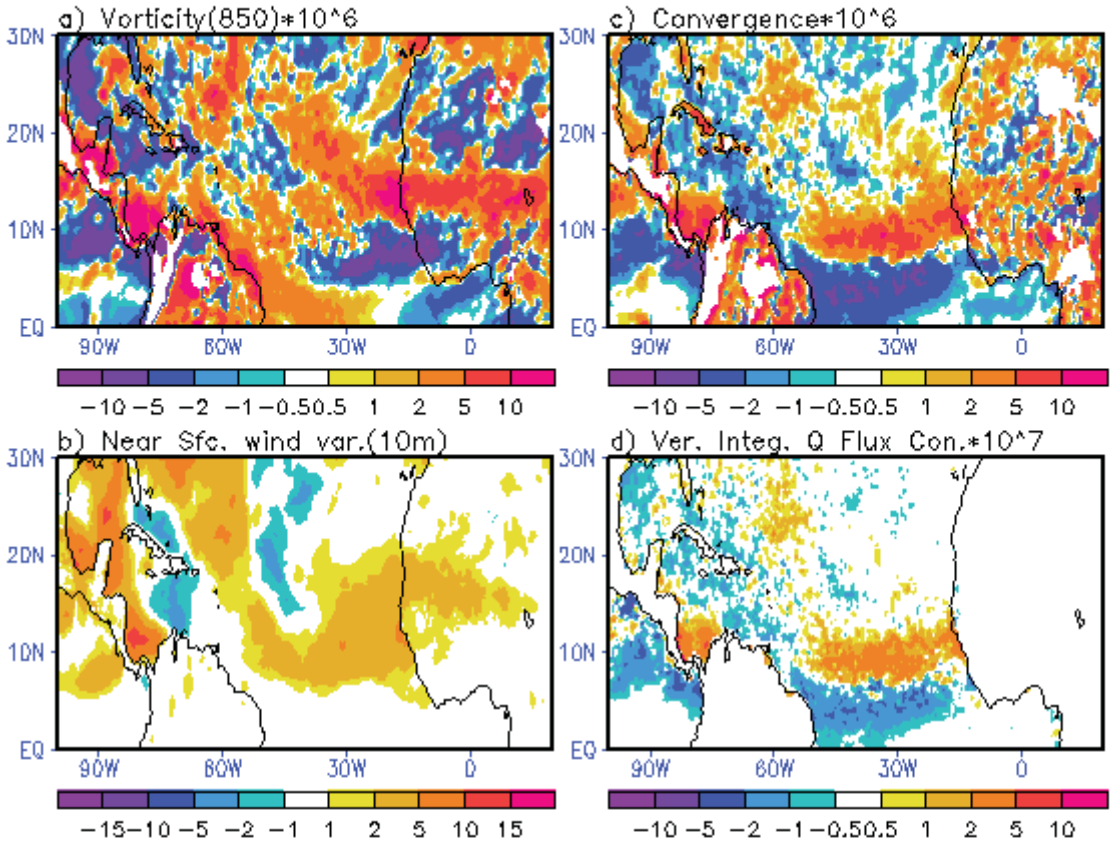

Figure 13. Difference in a) relative vorticity at 850hP, b) wind variance at 10m level, c) convergence at 925hPa and d) vertically integrated moisture flux convergence between ExpA and ExpC (ExpA minus ExpC) during hurricane season (June through November) of 2005.

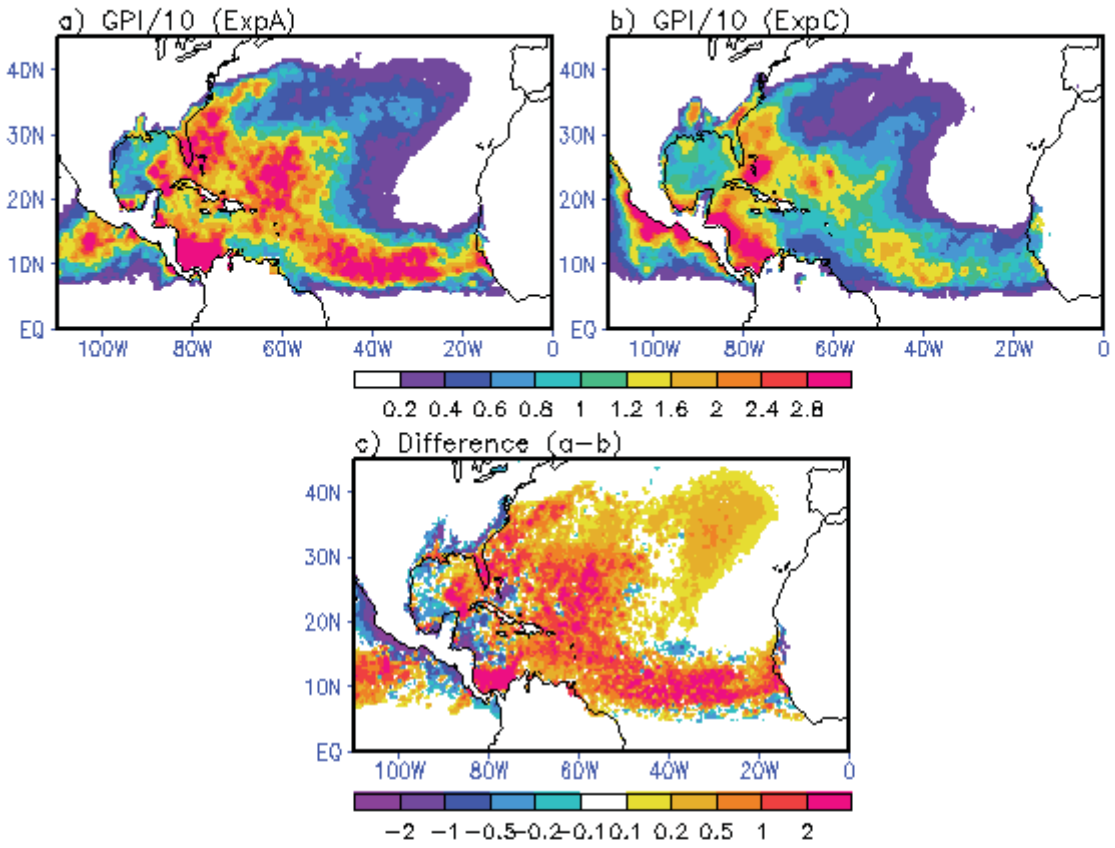

Figure 14. Distribution of modified genesis potential indices for 2005 from a) ExpA, b) ExpC and c) difference (ExpA minus ExpC)

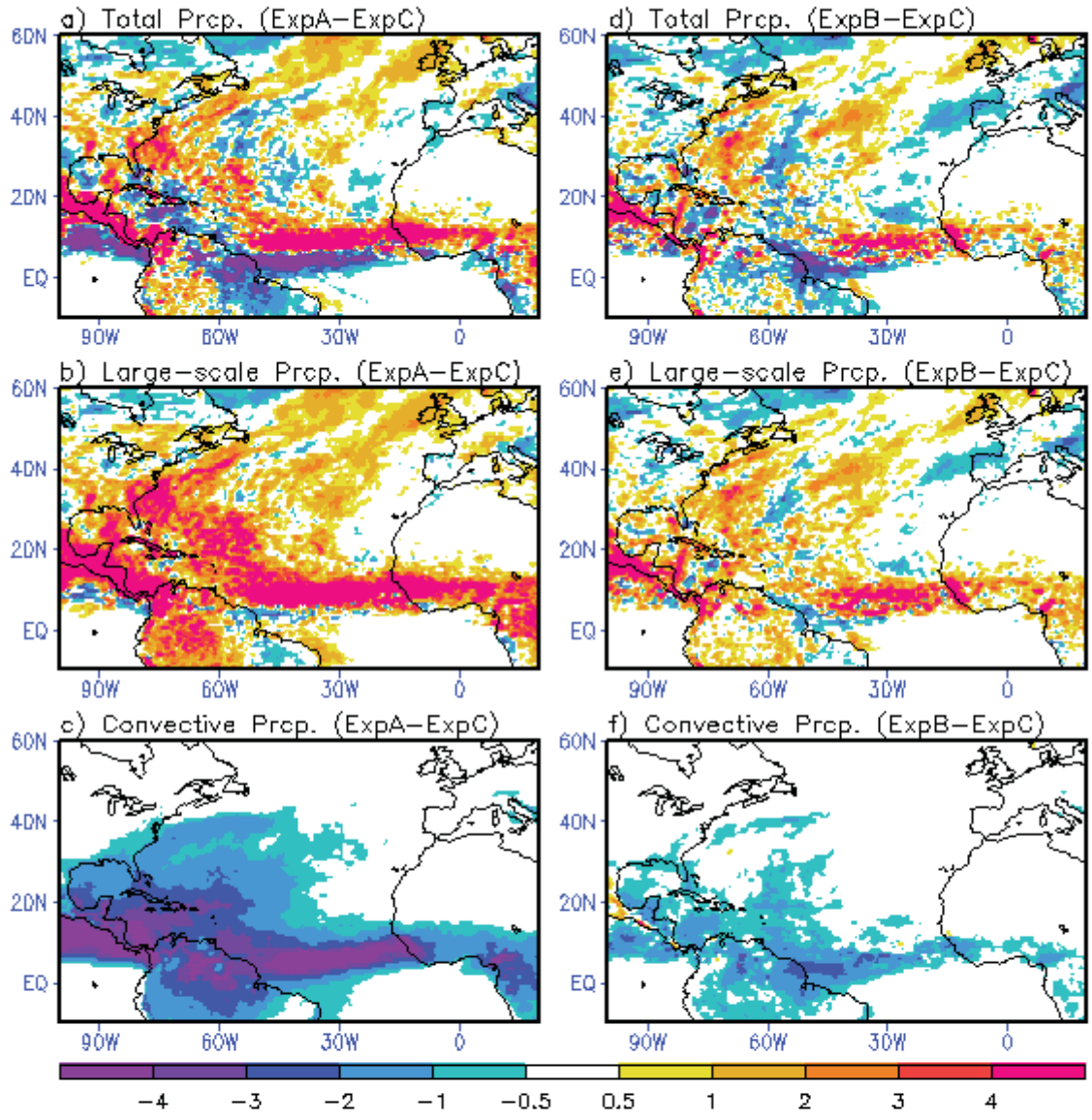

Figure 15. Difference in a) total precipitation, b) large-scale precipitation and c) convective precipitation between ExpA and ExpC (ExpA minus ExpC) during 2005 hurricane season. Right panel is the same as the left panel but for difference between ExpB and ExpC (ExpB minus ExpC).

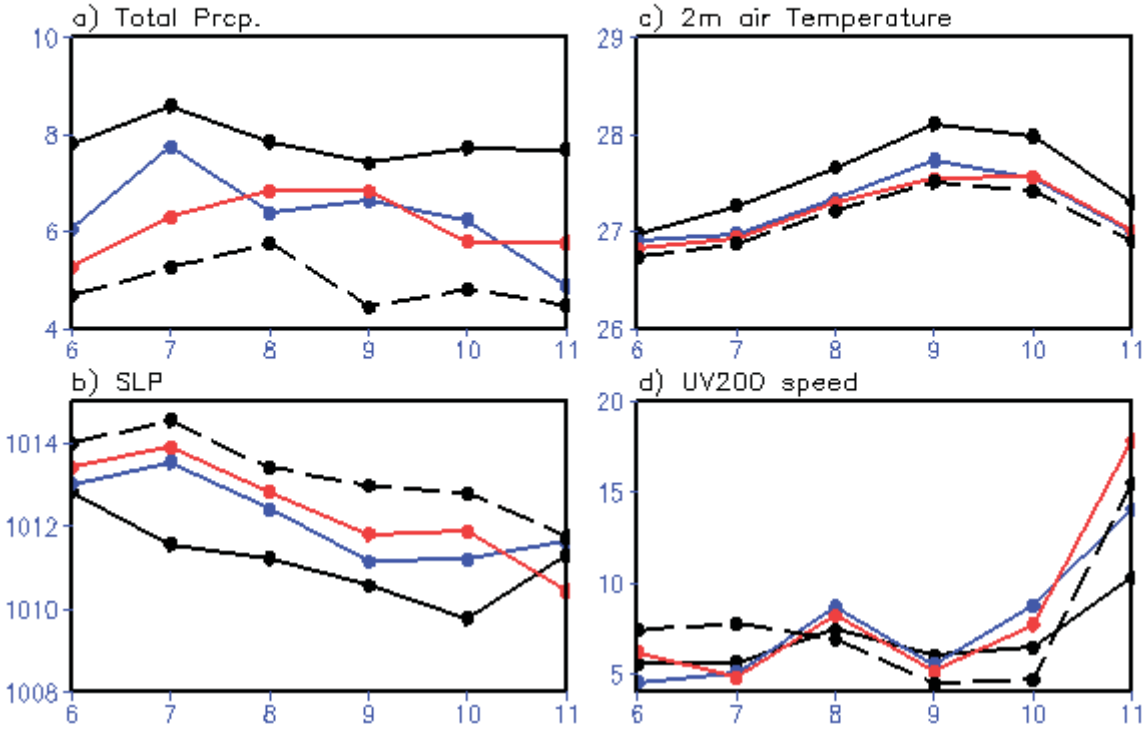

Figure 16. The seasonal variation of the area-averaged a) total precipitation, b) SLP, c) 2m air temperature and d) 200hPa wind speed for 2005. The geographical domain for area-averaging covers the typical TC genesis region over the Atlantic that spans 60°W-15°W, 5°N-20°N. Black, blue, and red solid lines represent the results from ExpA, ExpB and ExpC, respectively. The observed (GPCP) precipitation and remaining variables from MERRA are plotted with black dashed lines.